# Chapter 3

# Traveling Wave based Primary Protection and Fault Localization Scheme for MTDC Grid Considering IEC 61869-9 Measurement Standard

## 3.1 General

### 3.1.1 Brief Introduction

HVDC transmission systems are commonly used to integrate renewable energy sources such as offshore and onshore wind farms to conventional HVAC grids. Moreover, the HVDC transmission systems have several other benefits over HVAC transmission systems such as large electrical power transfer capability over long distances, interconnecting asynchronous AC grids and independent active and reactive power control capability [103]. Generally, VSC are preferred over LCC in HVDC transmission system, as VSC HVDC system provides several advantages such as DC power flow reversal without changing DC voltage polarity, weak AC grid integration capability, black start capability and ability to extend two terminal DC transmission line to MTDC network. Nowadays, a MMC topology, a type of VSC converter, is used in MTDC transmission system with benefits such as high modularity, high efficiency and low switching frequency. Majorly, the MMC-MTDC transmission can be classified into two categories, half bridge MMC (HBMMC) and full

bridge MMC (FBMMC) MTDC transmission system. The FBMMC-MTDC grid have the DC fault blocking as well as DC fault ride through capability which does not require blocking of FBMMC converter [31]. Whereas, the HBMMC-MTDC grid does not have the DC fault blocking capability, as the fault current will pass from the AC side to the DC side via freewheeling diode of HBMMC converter. And therefore, HBMMC-MTDC grid would need a separate DC protection relaying and DCCB unit to detect and isolate faulty DC transmission line [32].

### 3.1.2 Motivation and Incitement

Much of the reported research on the TW-based DC fault detection and localization scheme discusses the conceptual aspects, but overlook important practical factors such as sampling frequency, computational time and communication/measurement compliance. There are very few studies on the practical applicability of TW-based protection and fault localization scheme of MTDC grid in the context of signal measurements and exchange limitations within DC substation. In general, IEC-61869-9 measurement and IEC-61850-9-2 communication protocol is used for the protection and control scheme incorporation within the DC substation [104]. The IEC-61850-9-2 protocol defines the detailed layered communication architecture within DC substation unit. And IEC-61869-9 protocol, replacing IEC 60044-8 digital solution, provide measurement standard for the instrument transformers for digital interface according to IEC-61850-9-2 communication standards. For an effective time-critical application such as DC protection and control unit, it uses IEC-61588 precision time protocol (PTP) for precise time synchronization (within 30 - 50 $ns$) among various local and neighbouring DC substation equipment's measured data [105]. In IEC-61869-9 measurement standards, the most relevant conformance classes for DC substation units are class A, which defines minimal service set required to transmit measured data via sample value (SV), and class B which defines the minimal service set required to support SV and generic object oriented substation event (GOOSE) message.

The IEC-61869-9 measurement protocol has upgraded the maximum sampling frequency measurement to 96 kHz for HVDC application. But several single as well as double-ended TW based primary protection and DC fault localization scheme in the literature uses high sampling frequency measurement (500 kHz-1 MHz) for accurate fault

localization, which limits their practical implementation and compliance to IEC-61869-9 measurement standards. In [38], a transient feature extraction based current differential protection scheme for MTDC grid is discussed, which is compliant to DC substation measurement protocol. But, it does not extract TWAT of the fault induced TW and therefore it can not locate the DC fault in the MTDC grid. The machine learning based MTDC protection and fault localization scheme [41, 47, 48] could be compliant to measurement standards in DC substation. But, it has not been deployed in real-world due to limited scalability, detailed system modelling requirements, intensive training for different fault conditions and system topology dependence. The TWAT based fault localization schemes [50, 51] are the most reliable, but they are not be compliant with IEC-61869-9 measurement standard. Moreover, most of the reported research has covered primary protection and offline fault localization objectives separately and non-coherently. Therefore, there is a requirement of reliable and comprehensive TWAT based primary protection and real time fault localization scheme for MTDC grid which could also be compliant with IEC-61869-9 measurement standards.

### 3.1.3 Contribution

The main contributions of the chapter are mentioned below -

1. Development of comprehensive TWAT based DC protection scheme, which include fault detection (discrimination between external fault/disturbance and internal fault) and real-time fault localization.

2. The focus of the work is centered around low sampling frequency (50 kHz) TWAT based primary protection and DC fault localization algorithm, which follows IEC-61869-9 measurement standard in a practical smart DC substation unit employing IEC-61850-9-2 protocol based communication architecture. The proposed scheme requires low-cost DC voltage sensor and inexpensive signal processing core with small data storage due to low sampling frequency requirement.

3. It provides enhanced robustness against wide variation in fault parameters (fault resistance, fault location, fault types), grid parameters, external fault, measurement noise, sampling frequency, time synchronization error and communication delay.

4. A low cost hardware intelligent electronics device (IED) based on DSP board Texas instrument (TI) TMS320F28379D is developed for proposed DC protection and fault localization scheme. And its real-time control hardware in loop (CHIL) validation is demonstrated for a CIGRE benchmark MTDC grid on a real time digital simulation (RTDS) platform.

## 3.2 Methodologies of Proposed Primary Protection and Fault Localization Algorithm

### 3.2.1 Processing of the Relaying Input Signal

Prior to estimating AT of the first incident fault induced TW, it is prudent to pre-process DC voltage signal (relay input signal) to eliminate any mutual coupling between DC positive and negative pole voltage using (3.1) as shown below [36] -

$$\begin{bmatrix} v_{m0} \\ v_{m1} \end{bmatrix} = \frac{1}{\sqrt{2}} \begin{bmatrix} 1 & 1 \\ 1 & -1 \end{bmatrix}^{-1} \begin{bmatrix} v_p \\ v_n \end{bmatrix} \tag{3.1}$$

Here, $v_{m0}$ and $v_{m1}$ are the mode-0 and mode-1 DC voltage respectively, whereas $v_p$ and $v_n$ are the positive and negative DC pole voltage at the terminal end of DC transmission line or cable. Out of which, only $v_{m1}$ is used as the relaying input signal for AT estimation of the fault induced TW [106].

### 3.2.2 Low Sampling Frequency AT Estimation of TW using Modified MM Gradient and Linear Regression Tool

Considering high speed DC relaying requirement for the MTDC transmission system, the method for estimating AT of the TW must be simple and computationally inexpensive. The MM technique is a suitable time domain based signal processing tool to detect signal's singular point, which is essential in TWAT estimation, as compared to several time-frequency domain based signal processing method such as discrete or continuous wavelet transform [107]. The wavelet transform based methods satisfactorily removes white noise but it is less tolerant toward abnormal voltage spikes, but MM based signal processing tool is suitable for extracting feature from abnormal spikes and noise contaminated signal. Moreover, MM-based methods have fast and simple calculation, without using

multiplication and division operator, as compared to integral transform based methods (e.g., Wavelet transform) [108].

For better removal of positive and negative abnormal pulse disturbances, the mode-1 signal $v_{m1}$ is initially passed through denoising opening-closing-closing-opening (OCCO) MM filter denoted as $F$ [109], which is given by (3.2)-

$$F(v_{m1}(t)) = \{v_{m1} \circ (v_{m1} \bullet g)(t) + v_{m1}(t) \bullet (v_{m1} \circ g)(t)\}/2 \tag{3.2}$$

where $v_{m1}(x)$ $(0 \leq x \leq X)$ and $g(y)$ $(0 \leq y \leq Y)$ represents the limited mode-1 DC voltage signal and SE signal respectively. And $X$ and $Y$ are the moving window's length and SE's length. Apart from that, $\circ$ and $\bullet$ represents the open and close operator respectively in MM study, which are defined by (3.3) and (3.4) as -

$$(v_{m1} \circ g)(t) = (v_{m1} \ominus g \oplus g)(t) \tag{3.3}$$

$$(v_{m1} \bullet g)(t) = (v_{m1} \oplus g \ominus g)(t) \tag{3.4}$$

where $\ominus$ and $\oplus$ are the erosion and dilation operators respectively, which are defined by (3.5) and (3.6) as [110] -

$$(v_{m1} \ominus g)(t) = \min(v_{m1}(t+y) - g(y)) \tag{3.5}$$

$$(v_{m1} \oplus g)(t) = \max(v_{m1}(t-y) + g(y)) \tag{3.6}$$

Generally, the shape and length of SE affects the fault (pulse) detection sensitivity whose selection depends on anticipated transient signal [110]. In fact, the wave shape of the fault induced TW is quasi-step signal. Therefore, the flat shaped SE is used and the length of SE, i.e.; $M$ is taken as 3 to further reduce the computational delay of the proposed technique.

After that, MMG is applied to the OCCO filter output of (3.2) to estimate fault induced TWAT [108]. The MMG is denoted by $G$, which is given by (3.7) -

$$G(F(v_{m1}))(t) = (F(v_{m1}) \oplus g)(t) - (F(v_{m1}) \ominus g)(t) \tag{3.7}$$

The peak of modified MMG output of (3.7) corresponds to the estimated AT of fault induced TW with an error range of $\pm 1\mu s$ for the 1 MHz sampling frequency measurement. But, the performance of modified MMG output signal (3.7) will be poor for low sampling frequency measurement due to low time resolution. To upgrade the performance of MMG

output for lower sampling frequency application, the sobel operator and linear regression tool is further used in cascaded fashion. The sobel operator *sbl* is essentially a first order derivative used in MM study [111], which is defined as -

$$RS(t) = Sbl(G(F(v_{m1})))(t) = \frac{d(G(F(v_{m1})))(t)}{dt} \tag{3.8}$$

Where, $RS(t)$ is the DC relaying signal used to estimate TWAT of the fault induced TW. After first derivative operation of sobel operator, the TWAT (peak of $G(F(v_{m1}))(t)$) will corresponds to zero crossing point (ZCP) of the $RS(t)$ due to first derivative principle. But, the ZCP of DC relaying signal $RS(t)$ cannot be ascertained for lower sampling frequency measurement accurately. Therefore, linear regression tool is used to approximate the ZCP of $RS(t)$ for lower sampling frequency measurement, taking dispersed non-zero $RS(t)$ and time $t$ value as dependent and independent variable respectively. Therefore, the equation of linear regression algorithm can be formulated as -

$$RS_d(t) = b_0 + b_1 t + \varepsilon(t), \forall t \in (t_a, t_b) \tag{3.9}$$

Where $RS_d(t)$ is the time-indexed dispersed non-zero $RS(t)$ value, $t_b$ and $t_a$ are the end and starting timestamp value for the signal $RS_d(t)$. $b_0$ (constant) and $b_1$ (slope) are coefficients of the linear regression equation, whereas $\varepsilon$ is the linear regression error as shown in (3.9). Equation (3.9) can be written in matrix form as shown in (3.10) -

$$RS_d = xb + \in \tag{3.10}$$

where $RS_d = [RS(t_a), ....., RS(t_b)]^T$ is the matrix of time-indexed dispersed $RS(t)$ value, $b = [b_0, b_1]^T$ is the linear regression coefficient matrix, $\in = [\in (t_a), ....., \in (t_b)]^T$ is the error vector, and $x = \begin{bmatrix} 1 \ldots . 1 \\ t_a \ldots t_b \end{bmatrix}^T$ is the independent variable matrix. To estimate linear regression coefficients ($b_0$ and $b_1$) in (3.9), linear regression analysis tool which are based on least square estimation (LSE) [112], gradient descent [113] or singular value decomposition (SVD) [114] can be used. Out of these, LSE based linear regression technique is selected to estimate regression coefficients due to its efficient computation speed and simplistic linear algebraic equation based approach. It is used to estimate regression coefficient by solving -

$$min_{b_0, b_1}(RS_d - xb) \tag{3.11}$$

Since (3.10) is a linear equation set, therefore, the solution to (3.11) is

$$\hat{b} = (x^T x)^{-1} x^T R S_d \tag{3.12}$$

where $\hat{b} = [\hat{b}_0, \hat{b}_1]$ is the calculated linear regression coefficient, $(.)^T$ indicates transposition of matrix. Since $RS_d = 0$ at the ZCP, therefore AT can be estimated by solving $\hat{b}_0 + \hat{b}_1 t = 0$ and obtained as -

$$AT = -\frac{\hat{b}_0}{\hat{b}_1} \tag{3.13}$$

In summary, a three-step process is employed to estimate TWAT for low sampling frequency measurement. In the first step, a modified MMG technique is used to extract fault induced TW from DC voltage signal. But TWAT accuracy, which corresponds to peak of modified MM gradient output, is poor for low sampling frequency measurements. Therefore, the sobel operator is applied to the modified MMG output in the next step. Now, the new TWAT will correspond to the ZCP of sobel operator output. For accurate TWAT estimation, the linear regression technique extracts the precise ZCP (TWAT) of low sampling frequency measured sobel operator output signals in the third step.

The performance of modified MMG and proposed TWAT detection technique for the DC fault $F_1$ instigated TW is demonstrated in Fig. 3.1 for a two terminal DC transmission line (DC link between two MMC converter ($MMC_A$ and $MMC_B$) interfaced offshore wind farm platform) of a four terminal meshed MTDC grid as shown in Fig. 3.2 [115]. The sampling frequency measurement has been taken as 100 kHz to compare the performance of proposed TWAT estimation technique with modified MMG tool. A noise contaminated test DC voltage signal waveform with fault induced TW is shown in Fig. 3.1(a) and the TWAT determination of the TW using modified MMG technique is 0.700950 s as demonstrated in Fig. 3.1(b). While on the other hand, the proposed technique detects the TWAT (ZCP) of the TW as 0.7009638 s, as shown in Fig. 3.1(c), which is closer to the TWAT detection by the modified MMG technique with 1000 kHz, i.e.; 0.700964 s. The performance of proposed TWAT estimation method shown in Fig. 3.1(c) is better illustrated and summarized through block diagram as shown in Fig. 3.1(d), where the modified MMG output estimates TWAT to be 0.700950 s which is inaccurate due to low time resolution corresponding to low sampling frequency measurement. After that the MMG output is passed through sobel operator and linear regression tool, which estimates the accurate ZCP or TWAT as 0.70096381 s for low sampling frequency measurement as

shown in Fig. 3.1(d).

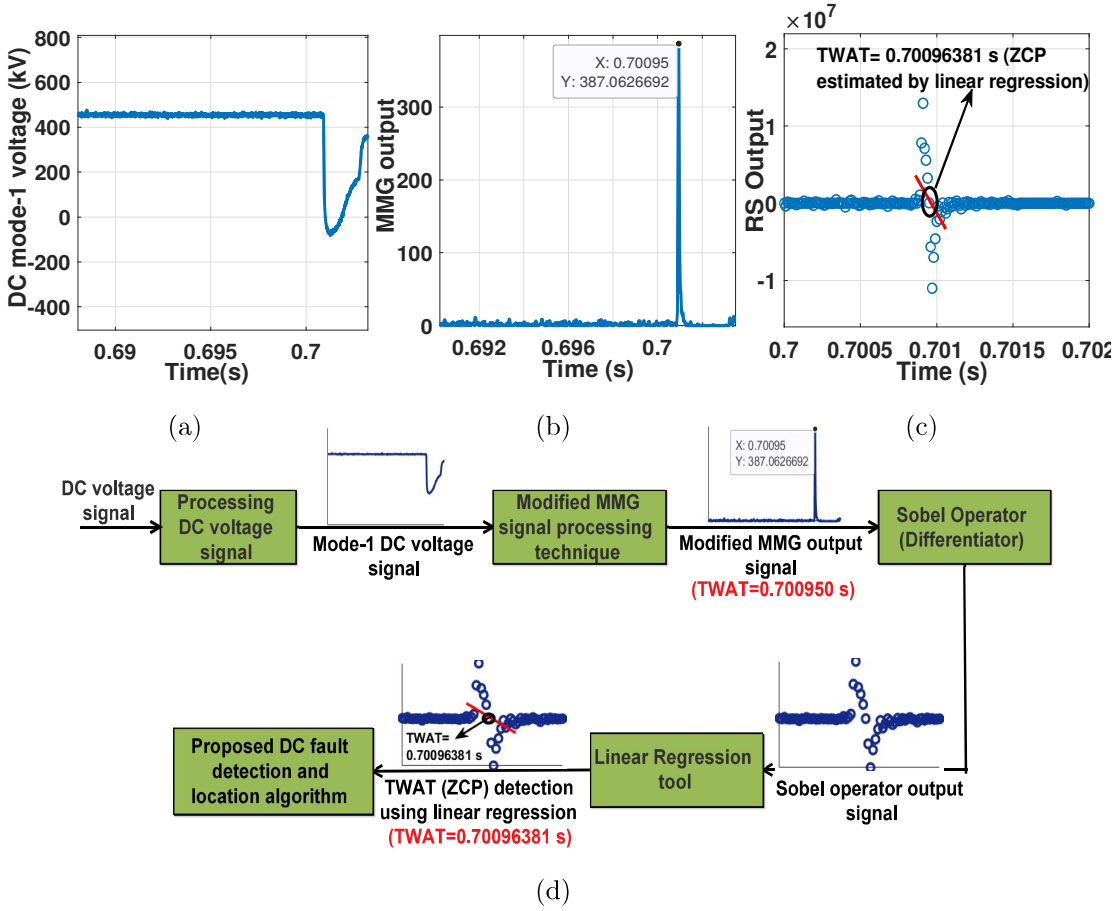


Figure 3.1: (a) Fault induced TW in DC voltage, (b) TWAT determination using modified MMG output, (c) Proposed technique (based on modified MMG,sobel operator and linear regression) based AT detection for TW for low sampling frequency measurement, (d) Block diagram illustration of the performance of proposed AT detection technique under low sampling frequency measurement.

Consider a DC fault $F_1$, at a distance $xl_{AB}$ from DC substation A, in DC link of length $L_{AB}$ as shown in Fig. 3.2. The TWAT at electrical potential transducer $PT_{AB}$ and $PT_{BA}$ will be -

$$AT_{AB} = t_0 + \frac{xl_{AB}}{v_{TW}} \tag{3.14}$$

$$AT_{AB} = t_0 + \frac{(1-x)l_{AB}}{v_{TW}} \tag{3.15}$$

Where $AT_{AB}$ and $AT_{AB}$ are the TWAT at $PT_{AB}$ and $PT_{BA}$ respectively. Here, $t_0$, $x$ and $v_{TW}$ are the fault inception time, per unit fault location value and velocity of mode-1

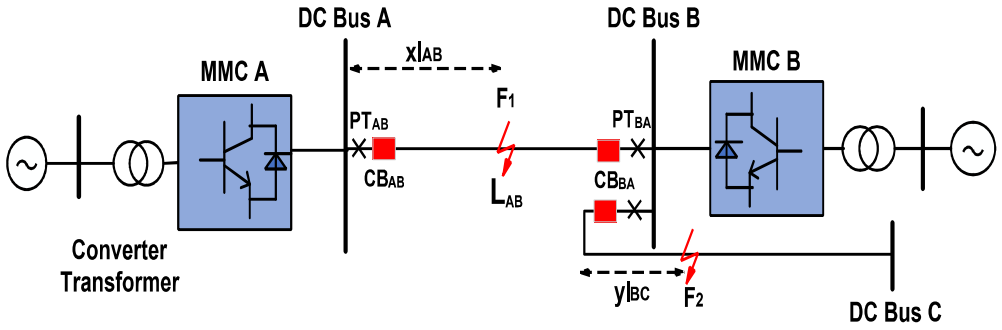


Figure 3.2: Two terminal DC link of MTDC transmission system.

TW in the DC transmission line. By combining the above equations, we get

$$AT_{AB} - AT_{BA} = \frac{(2x-1)l_{AB}}{v_{TW}} \tag{3.16}$$

Since $0 \leq x \geq 1$, therefore,

$$|AT_{AB} - AT_{BA}| < \frac{l_{AB}}{v_{TW}} \tag{3.17}$$

From (3.17), it can be concluded that if the TWAT difference between two DC link end is less than the TW propagation threshold of the protected DC link, then the fault is identified to be internal and a primary trip signal is sent to the associated HDCCB ($CB_{AB}$ and $CB_{BA}$). Since, the TWAT information is extracted using low sampling frequency measurement, the proposed TW based protection scheme will be compliant to IEC 61869-9 measurement standards. Similarly, an external DC fault $F_2$ is considered in DC cable of length $L_{BC}$ at a distance of $yl_{BC}$ from DC substation B. The TWAT estimation at $PT_{AB}$ and $PT_{BA}$ for the external fault will be -

$$AT_{AB} = t_0 + \frac{yl_{BC}}{v_{TW}} \tag{3.18}$$

$$AT_{AB} = t_0 + \frac{yl_{BC}}{v_{TW}} + \frac{l_{AB}}{v_{TW}} \tag{3.19}$$

Subtracting (3.18) from (3.19) and since $0 \leq y \geq 1$, we get -

$$|AT_{AB} - AT_{BA}| = \frac{l_{AB}}{v_{TW}} \tag{3.20}$$

Hence, if (3.20) is satisfied, then the fault is classified as an external fault.

Using the first incident TWAT information from both DC terminal ends, the calculated fault location (CFL) is formulated as -

$$CFL = (l - v_{TW}t_d)/2 \tag{3.21}$$

where $L$ is the transmission line length (km), $v_{TW}$ is the mode-1 traveling wave velocity (km/s) and $t_d = t_2 - t_1$ (s), in which $t_1$ and $t_2$ are the AT of the first incident TW at the DC terminal ends. The fault location error (FLE) can be formulated as -

$$FLE = \frac{|AFL - CFL|}{l} \times 100 \tag{3.22}$$

where $AFL$ is the actual fault location (km).

### 3.2.3 Flowchart of Proposed Primary Protection and DC fault Localization Scheme Compliant to IEC-61869-9 measurement protocol

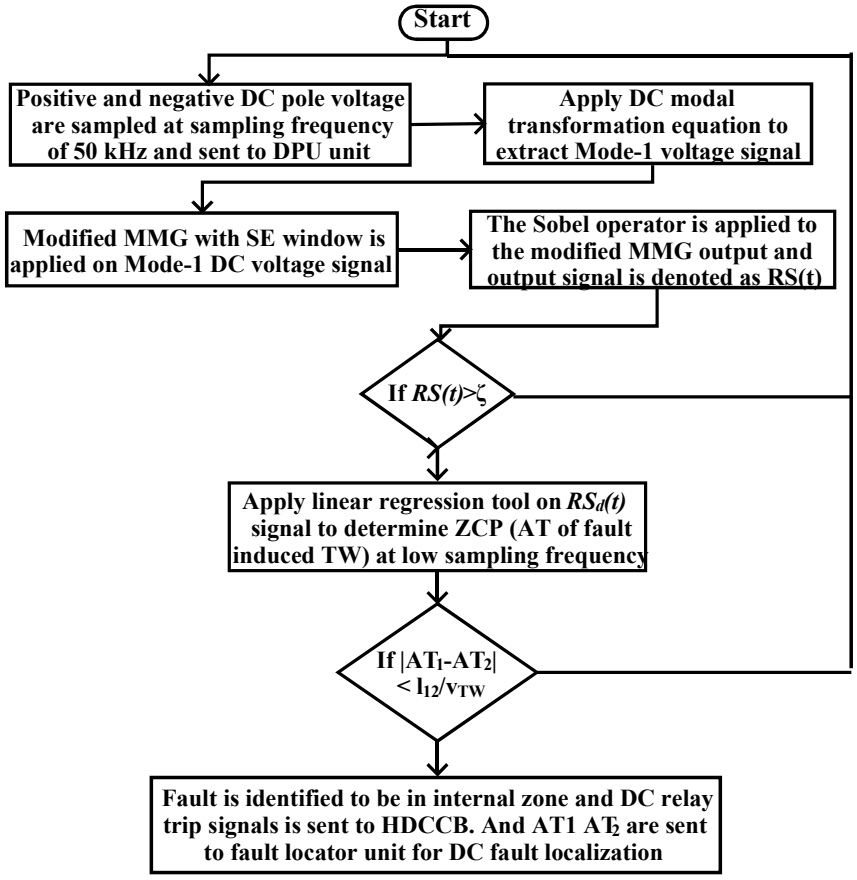


Figure 3.3: Flowchart of the proposed TW based primary protection and DC fault location algorithm compliant to IEC 61869-9 measurement protocol.

The computational flow of the proposed TW-based primary protection and fault location algorithm, compliant to IEC 61869-9 protocol, is shown in Fig. 3.3, which can be summarized as below -

1. The DC voltage sensors installed at DC line terminal ends will send DC pole voltage signals, compliant to IEC 61869-9 measurement protocol (50 kHz sampling frequency), to data processing unit (DPU). Here, DC modal transformation, modified MMG and sobel operator is applied to extract $RS(t)$ signal.

2. If $RS(t)$ signal exceeds the predetermined threshold $\zeta$, then linear regression tool is applied on the $RS_d(t)$ to determine ZCP (TWAT). Otherwise, go to step (1). The $\zeta$ for a test system is determined by the highest fault impedance and farthest located DC fault in the worst noise contaminated signal.

3. The AT of the first incident TW at the local and remote terminal (sent via optical communication link) are used to calculate TWAT difference. If the calculated TWAT difference is less than the TW propagation threshold of the protected line, then a primary relay trip signal is sent to associated HDCCB. Moreover, the TWAT information from DC terminal ends are also used to estimate real time fault location in DC fault locator unit.

## 3.3 MMC-MTDC Grid Under Study

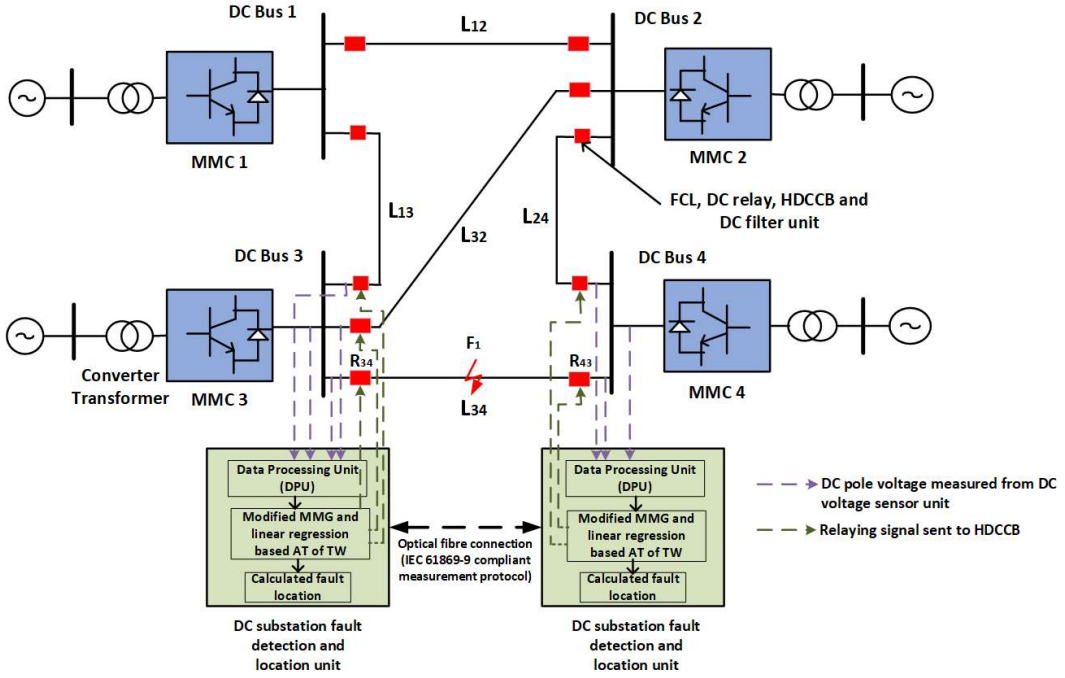


Figure 3.4: Test MTDC transmission system.

To verify the proposed DC protection and fault localization scheme's performance, a test meshed MMC-MTDC transmission system is used as shown in Fig. 3.4. It consists of two half bridge MMC converters (converter 1 and 3), connecting offshore wind farm, which feeds onshore AC grid with another two half bridge MMC converter (converter 2 and 4). The test MMC-MTDC system is modelled as symmetrical monopolar configuration with DC voltage of ± 320 kV. The MTDC grid consist of one DC link of 200 km ($L_{34}$), one DC link of 150 km ($L_{12}$), one DC link of 250 km ($L_{32}$) and two DC link of 100 km ($L_{13}$ and $L_{24}$). A DC bus reactor of 10 mH and HDCCB are also connected at the end of each DC link terminals. Further detailed parameters of the MMC converters and AC/DC grid system are tabulated in Table 3.1 [115].

Table 3.1: MMC converter and AC/DC grid parameters

| Converter and grid parameters | Converter 1,2,3 | Converter 4 |
|---|---|---|
| Rated power (MVA) | 900 | 1200 |
| AC grid voltage (kV) | 400 | 400 |
| DC grid voltage (kV) | ± 320 | ± 320 |
| AC converter voltage (kV) | 380 | 380 |
| AC grid reactance (Ω) | 17.7 | 13.4 |
| AC grid resistance (Ω) | 1.77 | 1.34 |
| Arm capacitance ($\mu F$) | 29.3 | 39 |
| Arm reactor (mH) | 84.8 | 63.6 |
| Arm resistance (Ω) | 0.885 | 0.67 |
| Bus filter reactor (mH) | 10 | 10 |

The DC substation primary protection and fault location unit comprises of DPU, which collects measured DC pole voltage from EPTs installed at the DC terminals. The pre-processing of relaying input signals are performed in local DPU unit using (3.1). In next step, the proposed TWAT estimation technique is used to determine fault induced TWAT at local DC terminal ends of transmission line. In general, IEC-61869-9 measurement and IEC-61850-9-2 communication protocol is used for the protection and control application within the DC substation [104]. Since, TWAT information is extracted using low frequency (50 kHz) sampled data, the proposed scheme is compliant to IEC 61869-9

measurement protocol which limits the maximum allowable sampling frequency of 96 kHz for DC application. The TWAT data from the remote neighbouring DC terminal ends are exchanged as IEC-61850-9-2 GOOSE message via optical fiber communication link. For effective DC protection and fault localization operation, it uses IEC-61588 precision time protocol for time synchronization (within 30-50 $ns$) among various local and neighbouring DC substation EPT's measured data [105] to minimize the synchronization error effect. With synchronized TWAT information from both DC terminal ends, the DC fault location is calculated and a subsequent primary relaying trip signal is sent to respective HDCCB units of the DC link as shown in Fig. 3.4.

## 3.4 Simulation Results and Discussion

The PSCAD/EMTDC software is used to model the MMC-MTDC test system drawn in Fig. 3.4. The half bridge MMC converter is modelled using continuous equivalent MMC model with blocking/de-blocking capabilities. And the cables are modelled using frequency dependent (phase) model, which can accurately represent transient behavior of the meshed MMC-MTDC transmission system. The traveling wave propagation velocity in the DC cable is found to be 172.7 km/ms which is extracted from some known fault location and transient measurement in test MTDC system. The blocking signals of IGBTs are triggered by converter internal overcurrent and overvoltage protection unit to protect MMC converter unit. The simulation time step in PSCAD simulation and SNR in noise contaminated signal is taken as 20 $\mu s$ (50 kHz sampling frequency) and 35 dB respectively, unless stated otherwise. The predetermined threshold ($\zeta$) for the test system is found to be $\pm 0.5 \times 10^6$, which is empirically determined by simulating a 200 $\Omega$ (highest) fault resistance in DC cable $L_{34}$ at distance of 195 km (farthest located) from DC substation 3 under 35 dB SNR (worst) noise contaminated signal.

### 3.4.1 Impact of DC fault resistance

#### 3.4.1.1 Performance of proposed protection scheme

To exhibit the proposed DC fault detection scheme's performance against different fault resistances, a pole-to-pole (PP) fault with different fault resistances (10 $\Omega$, 100 $\Omega$, 200 $\Omega$)

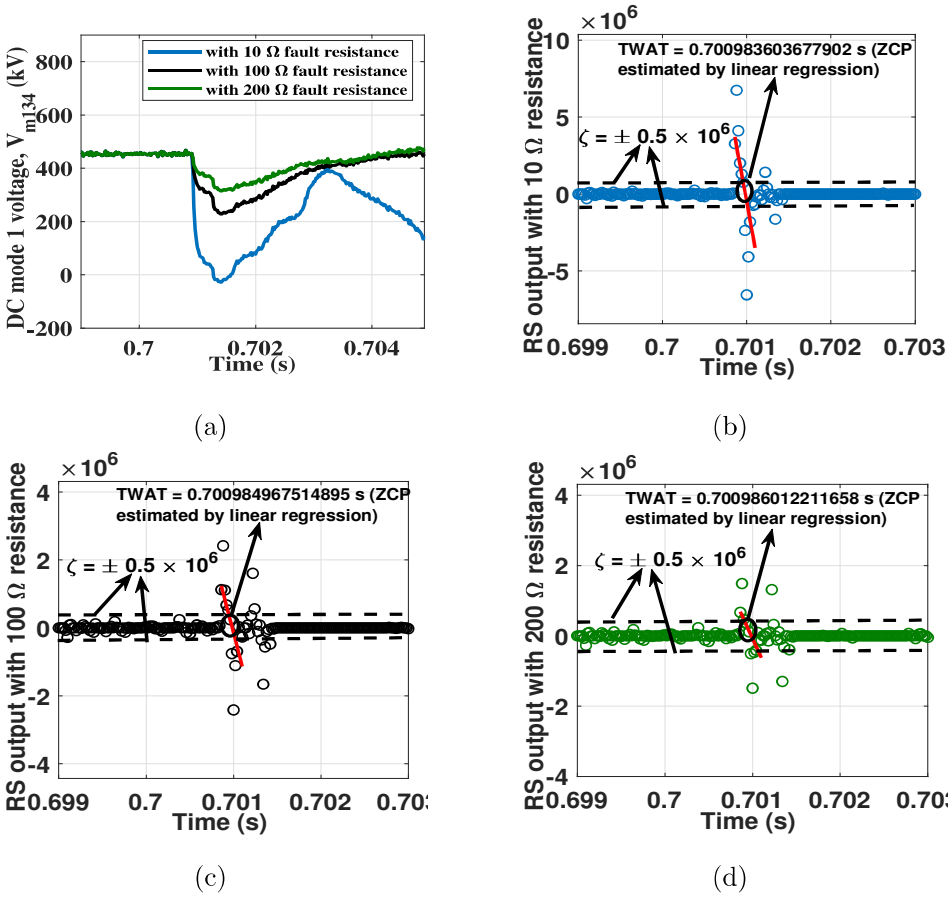


Figure 3.5: Measurement of EPTs at DC terminal 3 (a) Mode-1 DC voltage ($V_{m134}$ waveform with different fault resistance), (b) AT detection of 10 Ω fault resistance induced TW, (c) AT detection of 100 Ω resistance fault induced TW, (d) AT detection of 200 Ω resistance fault induced TW.

at 0.7 s are simulated in the DC link $L_{34}$ at 170 km distance from DC substation 3. As evident from Fig. 3.5 (b), (c) and (d), the threshold $\zeta = \pm 0.5 \times 10^6$ is used to discriminate between non-faulted event such as HDCCB opening on the neighbouring line and noise interference up to 35 dB from $PT_{34}$. If $RS(t)$ exceeds the threshold $\zeta$, then proposed scheme extracts first incident TWAT from the mode-1 DC voltage signal $V_{m134}$ as shown in Fig. 3.5(a). The extracted TWAT by the proposed scheme are 0.700983604 s (Fig. 3.5(b)), 0.700984967 s (Fig. 3.5(c)) and 0.700986012 s (Fig. 3.5(d)) for 10 Ω , 100 Ω and 200 Ω fault resistance respectively.

Similarly, the proposed technique will estimate the TWAT from EPT measuring $V_{m143}$ at remote DC terminal 4 for different fault resistances (10 Ω, 100 Ω, 200 Ω), which is

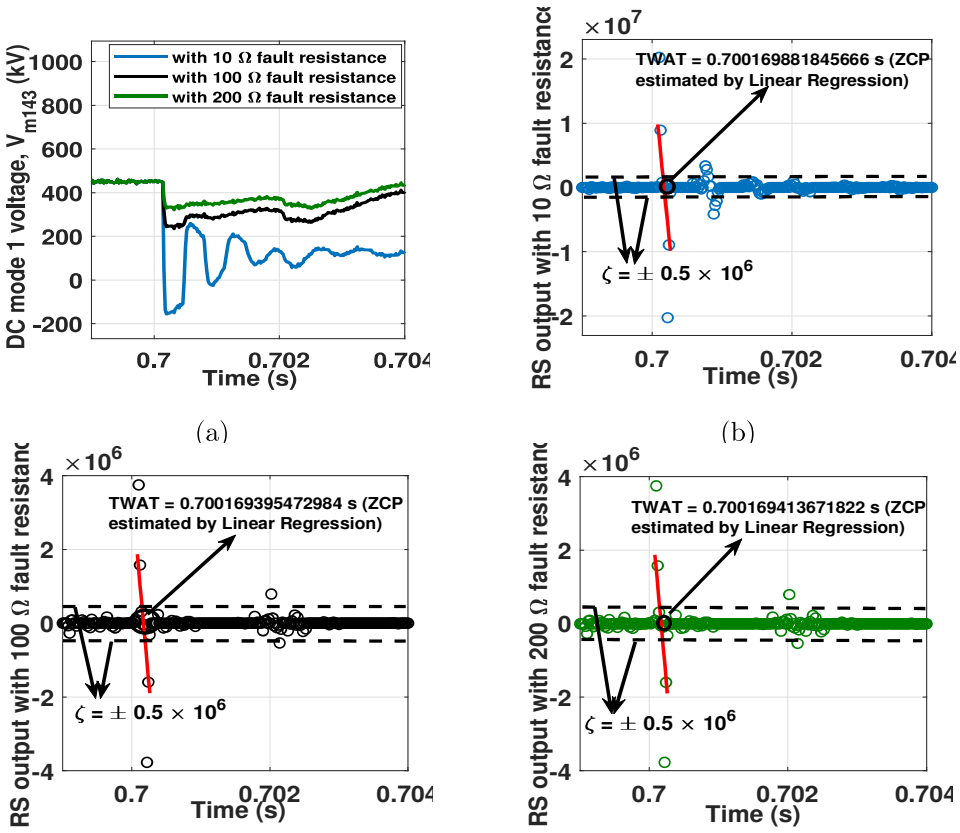


Figure 3.6: Measurement of EPTs at DC terminal 4 (a) Mode-1 DC voltage ($V_{m143}$ waveform with different fault resistance), (b) AT detection of 10 Ω fault resistance induced TW, (c) AT detection of 100 Ω resistance fault induced TW, (d) AT detection of 200 Ω resistance fault induced TW.

shown in Fig. 3.6(a). The estimated TWAT at DC terminal 4 is found to be 0.7001698818 s (Fig. 3.6(b)) for 10 Ω, 0.70016939547 s (Fig. 3.6(c)) for 100 Ω and 0.70016941367 s (Fig. 3.6(d)) for 200 Ω resistive fault. Table 3.2 summarizes and tabulates the TWAT information from DC terminal 3 and 4 for different fault resistance scenario shown in Fig. 3.5 and Fig. 3.6. As clearly evident from Table 3.2, the $|AT_{34} - AT_{43}|$ is always less than TW propagation threshold $\frac{L_{34}}{v_{TW}}$ for fault resistance up to 200 Ω, which identifies the fault to be in the internal zone for DC cable link $L_{34}$ and it sends the relay trip signal to $CB_{34}$ and $CB_{43}$. The proposed scheme detects and clear DC fault within 3-4 ms for the fault resistance up to 200 Ω as evident from mode-1 DC voltage at DC terminal 3 and DC current in $CB_{34}$ shown in Fig. 3.7(a) and (b) respectively. Since proposed

protection scheme uses 50 kHz sampled DC voltage sample, therefore it will be compliant to IEC-61859-9 measurement standard for DC fault resistance up to 200 Ω.

Table 3.2: Impact of fault resistance on proposed TW based protection scheme

| Fault resistance (Ω) | AT of TW at DC terminal 3, $AT_{34}$ (s) | AT of TW at DC terminal 4, $AT_{43}$ (s) | $(\lvert AT_{34} - AT_{43} \rvert)$ $(ms)$ | $\frac{l_{34}}{v_{TW}}$ $(ms)$ | Internal fault $(\lvert AT_{34} - AT_{43} \rvert) < \frac{L_{34}}{v_{TW}}$ |
|---|---|---|---|---|---|
| 10 | 0.700983604 | 0.7001698818 | 0.81372 | 1.1581 | Yes |
| 100 | 0.700984967 | 0.7001693955 | 0.81557 | 1.1581 | Yes |
| 200 | 0.700986012 | 0.7001694137 | 0.81660 | 1.1581 | Yes |

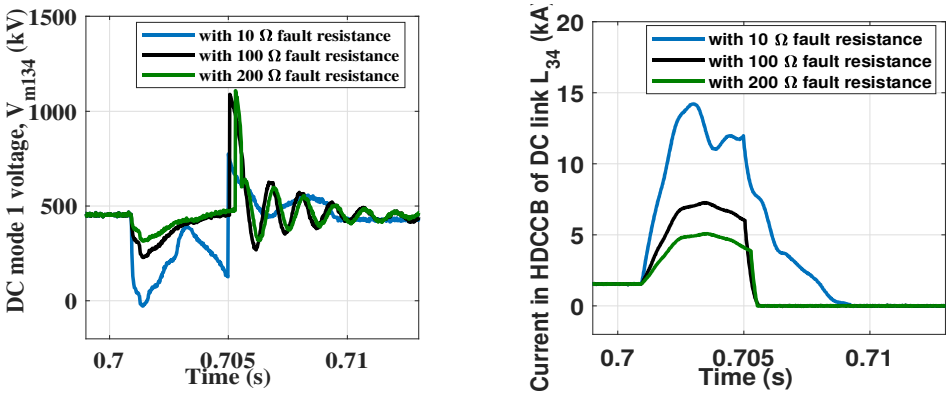


(a) (b)

Figure 3.7: (a) Mode-1 DC voltage of cable $L_{34}$ at DC terminal 3 with 10 Ω, 100 Ω and 200 Ω fault resistance, (b) Current in HDCCB of DC link $L_{34}$ for 10 Ω, 100 Ω and 200 Ω fault resistances.

#### 3.4.1.2 Performance of proposed fault localization scheme

To evaluate the performance of proposed DC fault localization scheme for different fault resistances, a PP fault with fault resistance of 10 Ω, 100 Ω and 200 Ω is simulated at a distance of 5 km, 60 km, 130 km and 190 km from DC substation 3 in DC cable link $L_{34}$. For that, the first incident TWAT estimated by proposed scheme at DC terminal 3 and 4

are tabulated in Table 3.3 to calculate real time DC fault location using (3.21). As evident from Table 3.3, FLE for the proposed fault localization scheme lies within the range of 0.750 % for fault resistance up to 200 Ω. Since the FLE estimated by the proposed TW based DC fault localization scheme lies within 1 % for low sampling frequency measured voltage sample, therefore it could be compliant to IEC-61869-9 measurement protocol.

Table 3.3: Impact of fault resistance on proposed TW based DC fault localization scheme

| AFL (km) | Fault re-sistance (Ω) | AT of TW at DC terminal 3, $AT_{34}$ (s) | AT of TW at DC terminal 4, $AT_{43}$ (s) | CFL (km) | FLE (%) |
|---|---|---|---|---|---|
| 20 | 10 | 0.7001162184 | 0.7010260107 | 21.44 | 0.719 |
| 20 | 100 | 0.7001157831 | 0.7010256183 | 21.44 | 0.719 |
| 20 | 200 | 0.7001156265 | 0.7010258217 | 21.40 | 0.702 |
| 60 | 10 | 0.7003505519 | 0.7008129348 | 60.07 | 0.035 |
| 60 | 100 | 0.7003496523 | 0.7008127921 | 60.01 | 0.005 |
| 60 | 200 | 0.7003506846 | 0.7008148724 | 59.92 | 0.040 |
| 130 | 10 | 0.7007527475 | 0.7004107306 | 129.53 | 0.235 |
| 130 | 100 | 0.7007533185 | 0.7004114276 | 129.52 | 0.240 |
| 130 | 200 | 0.7007529454 | 0.7004107628 | 129.55 | 0.225 |
| 190 | 10 | 0.7011112103 | 0.70008616328 | 188.51 | 0.744 |
| 190 | 100 | 0.7011107247 | 0.70008563821 | 188.52 | 0.742 |
| 190 | 200 | 0.7011114187 | 0.70008594820 | 188.49 | 0.755 |

Minimum FLE = 0.05 %, Maximum FLE = 0.755 %

Mean FLE = 0.430 %, Mean standard deviation = 0.318307 %

### 3.4.2 Impact of measurement noise and measurement error

#### 3.4.2.1 Impact of measurement noise

The EPTs installed ($PT_{34}$ and $PT_{43}$) at DC substations are susceptible to measurement noise. In general, signal to noise ratio (SNR) content of a typical EPT installed in HVDC project are found to be 34.99 dB [36], which may hinders the performance of proposed

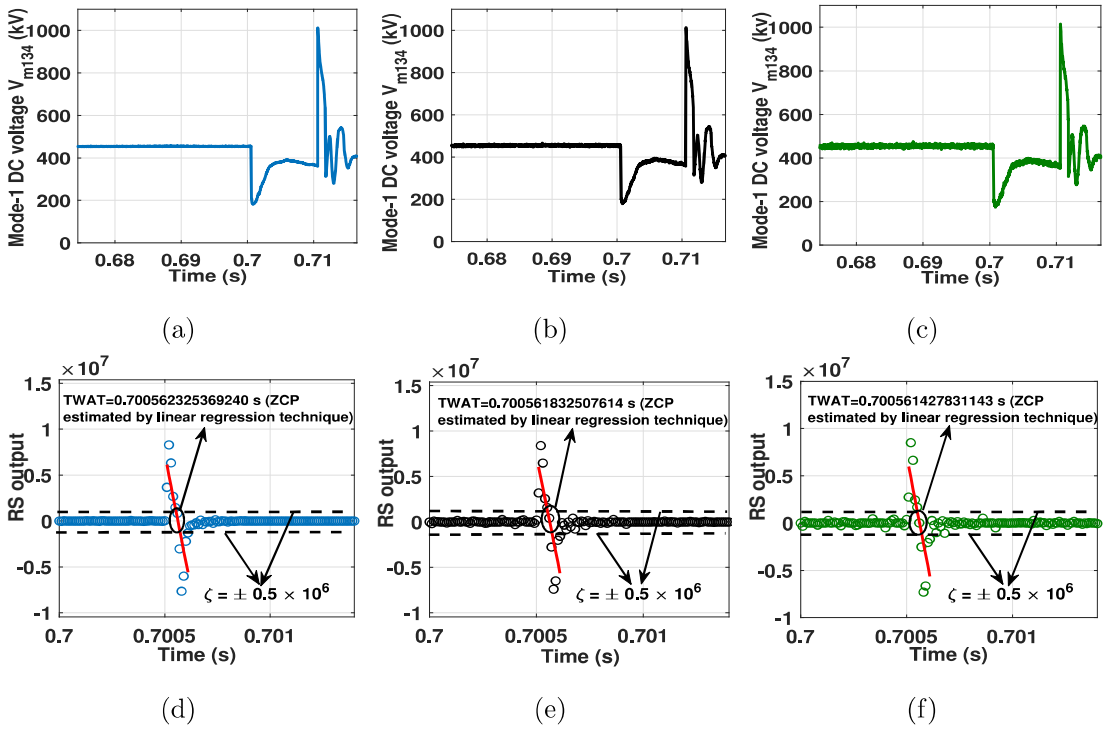


Figure 3.8: At DC terminal 3 (a) Mode-1 DC voltage with 55 dB SNR noise, (b) Mode-1 DC voltage with 45 dB SNR noise, (c)Mode-1 DC voltage with 35 dB SNR noise, (d) TWAT detection for 55 dB SNR contaminated DC voltage signal, (e) TWAT detection for 45 dB SNR contaminated DC voltage signal, (f) TWAT detection for 35 dB SNR contaminated DC voltage signal.

TWAT estimation technique. To study the effect of noise on the proposed TWAT detection and estimation technique, a PP fault with 50 Ω fault resistance is simulated in DC cable $L_{34}$ at distance of 100 km from DC substation 3. The efficiency of proposed TWAT detection algorithm is analyzed against 55 dB, 45 dB and 35 dB SNR noise contaminated DC voltage signal ($V_{m134}$) measured at $PT_{34}$, which is plotted in Fig. 3.8. As evident from Fig. 3.8, the proposed technique extracts TWAT as 0.700562 s, 0.700562 s and 0.700561 s for $V_{m134}$ signal contaminated with 55 db, 45 dB and 35 dB SNR respectively, which is consistent, accurate and insensitive to noise contamination. Similarly, the TWAT estimated by the proposed scheme at DC terminal 3 and 4 are tabulated in Table 3.4 to demonstrate the performance of proposed TW based primary protection and DC fault localization scheme. From Table 3.4, it is evident that the proposed TW based protection scheme correctly identifies the internal fault and FLE is estimated to be around 0.05 %

for noise contaminated DC voltage signal up to 35 dB SNR. Hence, it can be concluded that the proposed TW based primary protection and DC fault localization scheme will be more immune toward measurement noise up to 35 dB SNR.

Table 3.4: Impact of noise on proposed TW based protection scheme

| AT of TW at DC terminal 3, $AT_{34}$ (s) | AT of TW at DC terminal 4, $AT_{43}$ (s) | CFL (km) & FLE (%) | ($\lvert AT_{34} - AT_{43} \rvert$ ($ms$) | Noise (dB) | Internal fault ($\lvert AT_{34} - AT_{43} \rvert$) $< \frac{l_{34}}{v_{TW}}$ |
|---|---|---|---|---|---|
| 0.7005623253 | 0.7005629271 | 100.05 & 0.05 | 0.0006 | 55 | Yes |
| 0.7005618325 | 0.7005625316 | 100.05 & 0.05 | 0.0007 | 45 | Yes |
| 0.7005614278 | 0.7005621045 | 100.05 & 0.05 | 0.0007 | 35 | Yes |

#### 3.4.2.2 Impact of measurement error

The measurement error introduced by EPTs installed at the DC terminal might also effect the performance of proposed TWAT based protection and fault localization scheme. The impedance based protection and fault localization schemes requires positive ($Z_1$) and zero sequence impedance ($Z_0$) of the line parameters which are sensitive to measurement error introduced by EPTs and OCTs. Unlike impedance based protection and fault localization scheme, the TWAT based technique is not effect by measurement error in $Z_0$ and $Z_1$ HVAC system [116], and the same principle is being followed for HVDC system too. Albeit, the TWAT based protection and fault localization scheme depends on DC link length, sampling frequency and TW velocity. The TW velocity (172.7 km/s) in the DC transmission line depends on the sampling frequency (50 kHz) and frequency dependent line parameters ($L$ and $C$ measured from EPTs and OCTs) of the DC transmission line. The frequency dependent line parameters can be determined using [117], which depends on the voltage and current measurement at the DC terminal ends and are susceptible to

measurement error. The TW velocity with measurement error is given by -

$$(v_{TW} \pm \Delta v_{TW}) = \frac{1}{\sqrt{(L \pm \Delta L)(C \pm \Delta C)}}$$

To assess the performance of the proposed scheme, a 70 Ω PPG fault is simulated in DC link $L_{34}$ at a distance of 30 km and 130 km from DC substation 3 in the test MTDC system. The measurement error of ± 0.5 %, ± 0.75 % and ± 1 % is considered for DC link parameters $L$ and $C$, which will lead to TW velocity error margin of $\pm\Delta v_{TW}$ (± 0.5025 %, ± 0.756 % and ± 1.01 % respectively) and its effect on the performance of TW based protection and fault localization is tabulated in Table 3.5. As evident from Table 3.5, the proposed protection scheme correctly identifies the internal fault and maximum FLE is found to be less than the allowable limit of 1 % for measurement error up to 1 %.

Table 3.5: Impact of measurement error on proposed TW based DC protection and fault localization scheme

| AFL (km) | $\Delta L$ & $\Delta C$ (%) | $\Delta v_{TW}$ (%) | AT of TW at DC terminal 3, $AT_{34}$ (s) | AT of TW at DC terminal 4, $AT_{43}$ (s) | Internal fault ($\lvert AT_{34} - AT_{43}\rvert$) $< \frac{l_{34}}{v_{TW}}$ | Maxi--mum FLE (%) |
|---|---|---|---|---|---|---|
| 30 | ±0.5 | ±0.5025 | 0.7001695501 | 0.7009842947 | Yes | 0.355 |
| 30 | ±0.75 | ±0.756 | 0.7001695501 | 0.7009842947 | Yes | 0.442 |
| 30 | ±1 | ±1.01 | 0.7001695501 | 0.7009842947 | Yes | 0.533 |
| 130 | ±0.5 | ±0.5025 | 0.7007525502 | 0.7004111432 | Yes | 0..332 |
| 130 | ±0.75 | ±0.756 | 0.7007525502 | 0.7004111432 | Yes | 0.368 |
| 130 | ±1 | ±1.01 | 0.7007525502 | 0.7004111432 | Yes | 0.403 |

### 3.4.3 Impact of sampling frequency and fault location

#### 3.4.3.1 Performance of proposed protection scheme

The frequency dependent model of DC cable is modelled in PSCAD simulation environment for practical TW behavior covering wide frequency range, known as dispersion

effect [118]. The number of TW frequency component, velocity of TW ($v_{TW}$) and corresponding TW propagation threshold ($l_{34}/v_{TW}$) depends on the sampling frequency selection, which will be unique for every sampling frequency measurement. To evaluate the influence of fault location and sampling frequency on the proposed TW based protection scheme, a PP fault with 150 Ω fault resistance is simulated on DC link $L_{34}$ with increasing fault distance from 5 km to 195 km in a step size of 10 km. The simulation cases are performed with 500 kHz, 96 kHz and 50 kHz sampling frequency measurement and its corresponding $v_{TW}$ are 180.5 km/ms, 179.5 km/ms and 172.7 km/ms respectively. Consecutively, the TW propagation threshold ($l_{34}/v_{TW}$) is found to be 1.1078 ms, 1.1142 ms and 1.1581 ms for 500 kHz, 96 kHz and 50 kHz sampling frequency measurement respectively. The $|AT_{34} - AT_{43}|$ estimated by proposed TWAT detection scheme for PP fault in DC cable $l_{34}$ under different sampling frequency measurement scenarios is plotted in Fig. 3.9. As evident from Fig. 3.9(a), (b) and (c), the estimated $|AT_{34} - AT_{43}|$ is always less than the TW propagation threshold ($\frac{l_{34}}{v_{34}}$) 1.1078 ms, 1.1142 ms and 1.1581 ms for sampling frequency measurement up to 50 kHz, which satisfies primary protection criteria and sends a relay trip signal to associated HDCCBs ($CB_{34}$ and $CB_{43}$) of the protected DC cable $L_{34}$.

The time resolution is 20 $\mu s$ ($\Delta t$) for 50 kHz sampling frequency measurement and the maximum TWAT error for double ended TW fault location scheme will be 40 $\mu s$ ($2 \times \Delta t$) in a conventional TW based AT detection technique. But the proposed TWAT estimation scheme can estimate TWAT with accuracy up to 1 $\mu s$ even for low sampling frequency (50 kHz) measurement. A buffer TW propagation threshold and (3.20) condition is used for primary protection scheme instead of single TW propagation threshold to discriminate internal fault from an external fault. To check the resiliency of proposed TW based primary protection scheme against external fault, a positive pole to ground (PG) is simulated in DC link $L_{24}$, with varying distance from 5 km to 95 km in step size of 10 km, for 500 kHz, 96 kHz and 50 kHz sampling frequency measurement. The measured $|AT_{34} - AT_{43}|$ at DC substation 3 and 4 for an external fault in DC cable $L_{24}$, which lies within the buffer TW propagation threshold of $\frac{l_{34}}{v_{34}} \pm 1\mu s$ for sampling frequency measurement up to 50 kHz, is plotted as shown in Fig. 3.10, which satisfies (3.20) and makes it compliant to IEC-61869-9 standard.

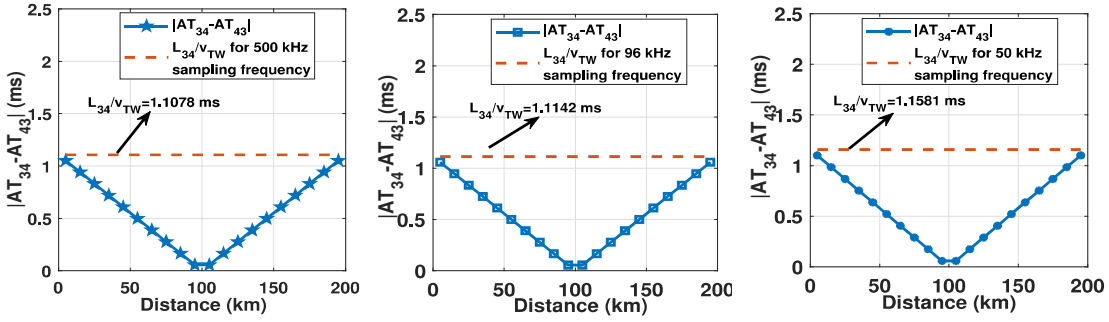


(a) (b) (c)

Figure 3.9: $|AT_{34} - AT43|$ estimation by the proposed protection scheme for 150 Ω DC fault in cable link $L_{34}$ with varying fault location (a) for 500 kHz sampling frequency, (b) for 96 kHz sampling frequency, (c) for 50 kHz sampling frequency.

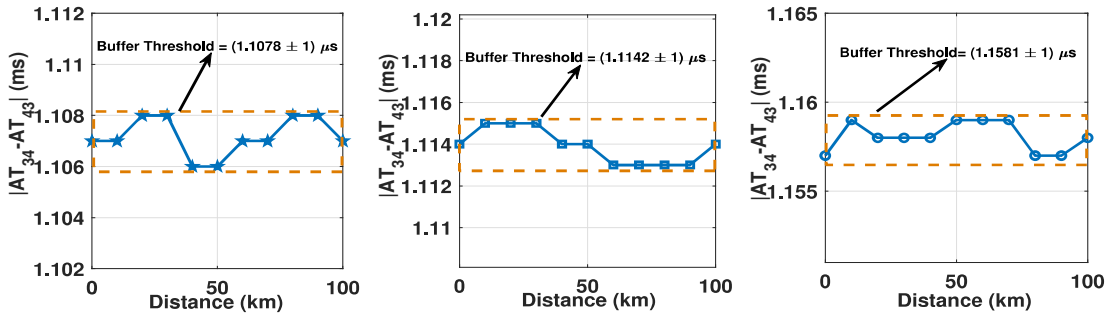


(a) (b) (c)

Figure 3.10: $|AT_{34} - AT43|$ estimation by the proposed protection scheme for 150 Ω DC fault in cable link $L_{42}$ with varying fault location (a) for 500 kHz sampling frequency, (b) for 96 kHz sampling frequency, (c) for 50 kHz sampling frequency.

#### 3.4.3.2 Performance of proposed fault localization scheme

The low sampling frequency measurement in conventional TW based DC fault localization corresponds to significant DC fault localization error due to lower time resolution. Furthermore, it is quite difficult to extract higher frequency component of TW for DC fault localization, because higher frequency components of TW are comparatively more attenuated than lower frequency component. Therefore, lower sampling frequency measurement based DC fault location schemes are prudent for the practical MTDC protection system, which are also compliant to IEC-61869-9 measurement protocol. A low sampling frequency TW based DC fault localization scheme which is compliant to IEC 61869-9 pro-

tocol uses using matrix pencil signal processing technique [119]. But it is not applicable for MTDC primary protection scheme due to high computational cost of matrix pencil technique. The proposed scheme uses computationally inexpensive TWAT extraction tool which are more suitable for DC protection and fault localization in MTDC grid [108].

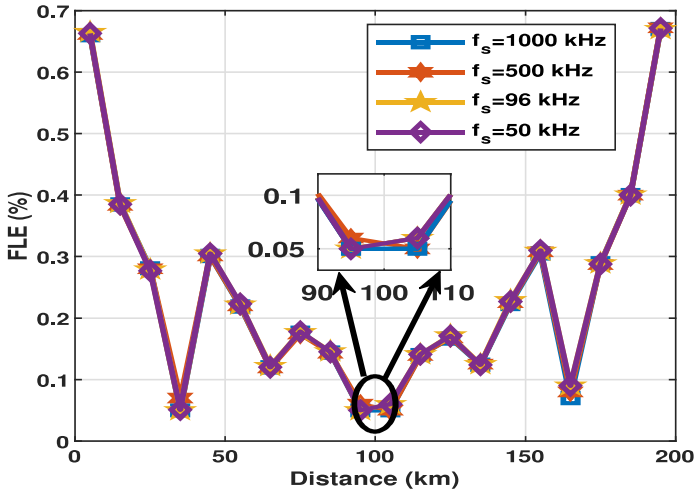


Figure 3.11: Impact of sampling frequency and fault location on proposed fault localization performance for fault on DC cable $L_{34}$.

To analyze the effect of sampling frequency and fault location on proposed fault localization technique, a PP fault with 100 Ω fault resistance is simulated in DC cable $L_{34}$ with varying distances from 5 km to 195 km from DC substation 3 with step size of 10 km. The calculated FLE from (3.22) is plotted for sampling frequency measurements of 500 kHz, 96 kHz and 50 kHz in Fig. 3.11. It is clear from Fig. 3.11 that FLE is always less than 0.750 %, even for 50 kHz sampling frequency which is compliant to IEC 61869-9 measurement protocol.

### 3.4.4 Impact of communication delay and synchronization error

#### 3.4.4.1 Impact of communication and signal processing delay on proposed primary protection scheme

One of the most prominent challenges in MTDC protection scheme is fast & timely detection and isolation of DC fault in MTDC grid. In general, the MTDC protection algorithm is expected to detect and isolate a DC fault within 1 - 2 $ms$ and 5 ms respectively. The total time delay ($t_{delay}$) needed by the proposed TW based protection scheme is given by

-

$$t_{delay} = t_{proc} + t_{comm} + t_{HDCCB} = t_{fltdet} + t_{HDCCB} \tag{3.23}$$

Where $t_{proc}$, $t_{comm}$, $t_{HDCCB}$ and $t_{fltdet}$ are the processing time of proposed TWAT detection technique, communication time delay, HDCCB opening time and fault detection time respectively. At first, the proposed TWAT estimation technique requires $t_{proc}$ delay to extract TWAT. It uses modified MMG (OCCO filter with MMG technique), sobel operator and linear regression tool, and the processing time delay to extarct TWAT is given by-

$$t_{proc} = t_{modMMG} + t_{sobel} + t_{linreg} \tag{3.24}$$

Where, $t_{modMMG}$, $t_{sobel}$ and $t_{linreg}$ are the processing time delay required by modified MMG, sobel operator and linear regression tool. Mathematically, each windowing operation of OCCO filter and MMG (modified MMG) requires $2 \times \Delta t \times (M-1)$ and $0.5 \times \Delta t \times (M-1)$ respectively [110]. In the proposed TW based protection scheme, the sampling time period ($\Delta t$) and length of SE ($M$) for MMG operation is selected as 20 $\mu s$ and 3 respectively. Therefore, the $t_{modMMG}$ is found to be 100 $\mu s$ as shown below -

$$\begin{aligned} t_{modMMG} &= (2 \times \Delta t \times (M-1)) + (0.5 \times \Delta t \times (M-1)) \\ &= (2 \times 20\ \mu s \times (3-1)) + (0.5 \times 20\ \mu s \times (3-1)) \\ &= 100\ \mu s \end{aligned} \tag{3.25}$$

In the next step, sobel operator is performed on the modified MMG output signal to get the DC relaying signal ($RS(t)$). It basically performs a differentiation operation and requires a time delay ($t_{sobel}$) of single time step ($\Delta t$) of 20 $\mu s$. After that, if the $RS(t)$ value exceeds the threshold $\zeta$, then the proposed TW based protection technique stores the dispersed 10 - 12 samples of $RS_d$ to extract ZCP (TWAT) which contributes to a time delay of $(10 \times \Delta t)$ to $(12 \times \Delta t)$. Finally, the linear regression tool extracts ZCP using (3.12) for small size matrices $RS_d$ and $x$ which needs an average low computational time of around 70 $\mu s$ in the MATLAB environment installed on a computer with Intel(R) Core(TM) i7-11800H processor and 16 GB RAM. So, the computation time for sobel operator and linear regression tool to extract ZCP will be -

$$\begin{aligned} t_{sobel} &= \Delta t = 20\ \mu s \\ t_{linreg} &= 12 \times \Delta t + 70\ \mu s = 190\ \mu s \end{aligned} \tag{3.26}$$

Substituting the computational time of $t_{modMMG}$, $t_{sobel}$ and $t_{linreg}$ from (3.25) and (3.26) in (3.24),

$$t_{proc} = 100\ \mu s + 20\ \mu s + 190\ \mu s = 310\ \mu s \tag{3.27}$$

The proposed double ended TW based protection scheme uses optical fiber based communication link between DC substation unit to exchange TWAT information via GOOSE messages, which will introduce a communication time delay ($t_{comm}$). It depends on the communication velocity ($v_{comm}$) and communication link length ($L_{AB}$) between DC substations (choosing DC substation 3 and 4), which is taken as 150 km/ms and 200 km respectively [120]. After receiving TWAT information from both DC terminal, (3.17) is used to send primary relay trip signal to the associated HDCCB which clears fault after time delay ($t_{HDCCB}$) of 2 $ms$. Summarily, the time delay $t_{comm}$ and $t_{HDCCB}$ is given as -

$$\begin{aligned} t_{comm} &= \frac{L_{AB}}{v_{comm}} = \frac{L_{34}}{v_{comm}} = 1.333\ ms \\ t_{HDCCB} &= 2\ ms \end{aligned} \tag{3.28}$$

Substituting the value of $t_{proc}$, $t_{comm}$ and $t_{HDCCB}$ from (3.27) and (3.28) in (3.23) will give $t_{fltdet}$ and $t_{delay}$ as 1.643 $ms$ and 3.643 $ms$ respectively, which is well within stipulated time frame of required MTDC protection requirement-

$$\begin{aligned} t_{fltdet} &= t_{proc} + t_{comm} \\ &= 0.310\ ms + 1.333\ ms = 1.643\ ms \\ t_{delay} &= t_{proc} + t_{comm} + t_{HDCCB} \\ &= 0.310\ ms + 1.333\ ms + 2\ ms \\ &= 3.643\ ms \end{aligned} \tag{3.29}$$

To evaluate the effect of communication delay on the proposed TW based protection scheme, a PP fault of 10 $\Omega$ fault resistance is simulated at 0.7 $s$ in DC link $L_{34}$ of test MTDC system. The proposed TW based protection scheme detects and clears DC fault by sending trip signal to HDCCBs $CB_{34}$ and $CB_{43}$. The DC fault is incepted at 0.7 $s$, but the fault induced TW will reach DC terminal 3 at 0.700500 $s$ and cleared DC fault at 0.704160 $s$ as evident from Fig. 3.12(a). Therefore the $t_{delay}$ introduced by the proposed protection scheme, which incorporates processing time of TW based AT estimation technique, communication delay and HDCCB opening delay, will be 3.66 $ms$

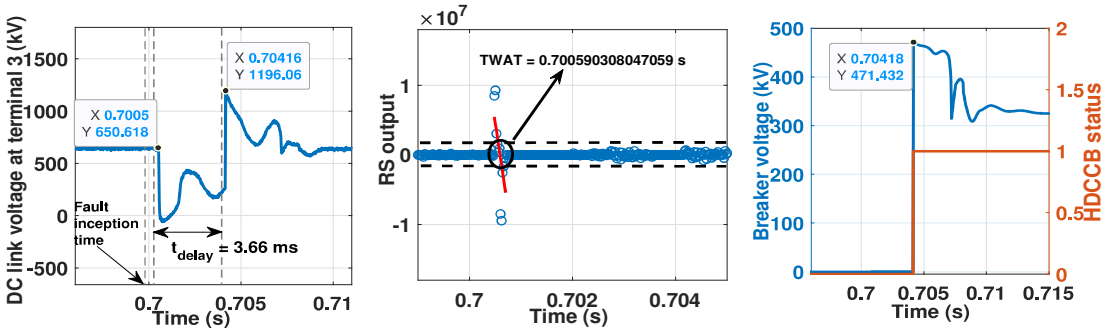


(a) (b) (c)

Figure 3.12: (a) Time stamps in transients of DC voltage waveform at DC terminal 3, (b) TWAT estimation by the proposed TWAT extraction technique, (c) HDCCB clearing DC fault and recovering DC pole voltage.

which is less than the required time frame of 5 $ms$ for MTDC primary protection scheme

-

$$t_{delay} = 0.704160\ s - 0.700500\ s = 3.66\ ms$$

The extracted TWAT at DC terminal 3 is found to be 0.7005903080 $s$ as shown in Fig. 3.12(b) which is communicated over optical fiber to DC terminal 4. As evident from Fig. 3.12(c), the proposed scheme clears DC fault at 0.704180 $s$, and the status of HDCCB changes from 0 to 1 and voltage across positive pole HDCCB recovered to 320 $kV$ consecutively.

#### 3.4.4.2 Impact of synchronization error on proposed real time fault localization scheme

The time precision of the synchronized measurement at two DC terminal ends are paramount to ensure accurate DC fault localization. Any time deviation in the synchronized measurement at DC terminal ends could lead to significantly large fault location error. In this subsection, the effect of time synchronization error on the proposed DC fault localization scheme is studied.

In general, DC substation protection and control architecture uses IEC-61869-9 measurement and IEC-61850-9-2 communication protocol [104]. For effective time critical application such as proposed TW based protection and fault localization scheme, it uses IEC-61588 PTP for precision time synchronization within 30 - 50 $ns$ among various local

Table 3.6: Impact of $\Delta t_{syn}$ on proposed TW based DC fault localization scheme

| AFL (km) | $\Delta t_{syn}$ ($\mu s$) | AT of TW at DC terminal 3, $AT_{34}$ (s) | AT of TW at DC terminal 4, $AT_{43}$ (s) | CFL (km) | FLE (%) |
|---|---|---|---|---|---|
| 30 | 1 | 0.7001698649 | 0.7009847223 | 29.63 | 0.19 |
| 30 | 2 | 0.7001698649 | 0.7009857223 | 29.55 | 0.23 |
| 30 | 3 | 0.7001698649 | 0.7009867223 | 29.46 | 0.27 |
| 30 | 4 | 0.7001698649 | 0.7009877223 | 29.38 | 0.31 |
| 30 | 5 | 0.7001698649 | 0.7009887223 | 29.29 | 0.36 |
| 140 | 1 | 0.7008122467 | 0.7003612350 | 138.94 | 0.53 |
| 140 | 2 | 0.7008122467 | 0.7003622350 | 138.85 | 0.58 |
| 140 | 3 | 0.7008122467 | 0.7003632350 | 138.77 | 0.62 |
| 140 | 4 | 0.7008122467 | 0.7003642350 | 138.69 | 0.66 |
| 140 | 5 | 0.7008122467 | 0.7003652350 | 138.60 | 0.70 |

and neighbouring DC substation unit [105]. In order to access the influence of synchronization error on proposed fault localization scheme, the time synchronization error ($\Delta t_{syn}$) is taken as 1 $\mu s$, 2 $\mu s$, 3 $\mu s$, 4 $\mu s$ and 5 $\mu s$ at DC terminal 3 measured voltage sample. And the its performance against time synchronization error ($\Delta t_{syn}$) for a PPG fault in DC cable $L_{34}$ at 30 km and 140 km distance from DC terminal 3 is tabulated in Table 3.6. Although the proposed scheme uses IEC-61588 PTP protocol which ensures maximum $\Delta t_{syn}$ of 50 $ns$, its performance is evaluated for $\Delta t_{syn}$ up to 5 $\mu s$ and estimated fault location error lies within 1 %. as shown in Table 3.6.

### 3.4.5 Impact of fault type

To study the impact of fault type on the proposed TW based protection and fault localization scheme, a positive pole-to-ground (PPG), negative PG (NPG) and pole-to-pole-to (PP) fault with 20 Ω fault resistance is simulated on the DC cable $L_{34}$ at a distance of 70 $km$ from DC substation 3. The measured mode-1 DC voltage waveform at DC terminal 3 for PPG, positive PG and negative PG fault is shown in Fig. 3.13(a), (b) and (c)

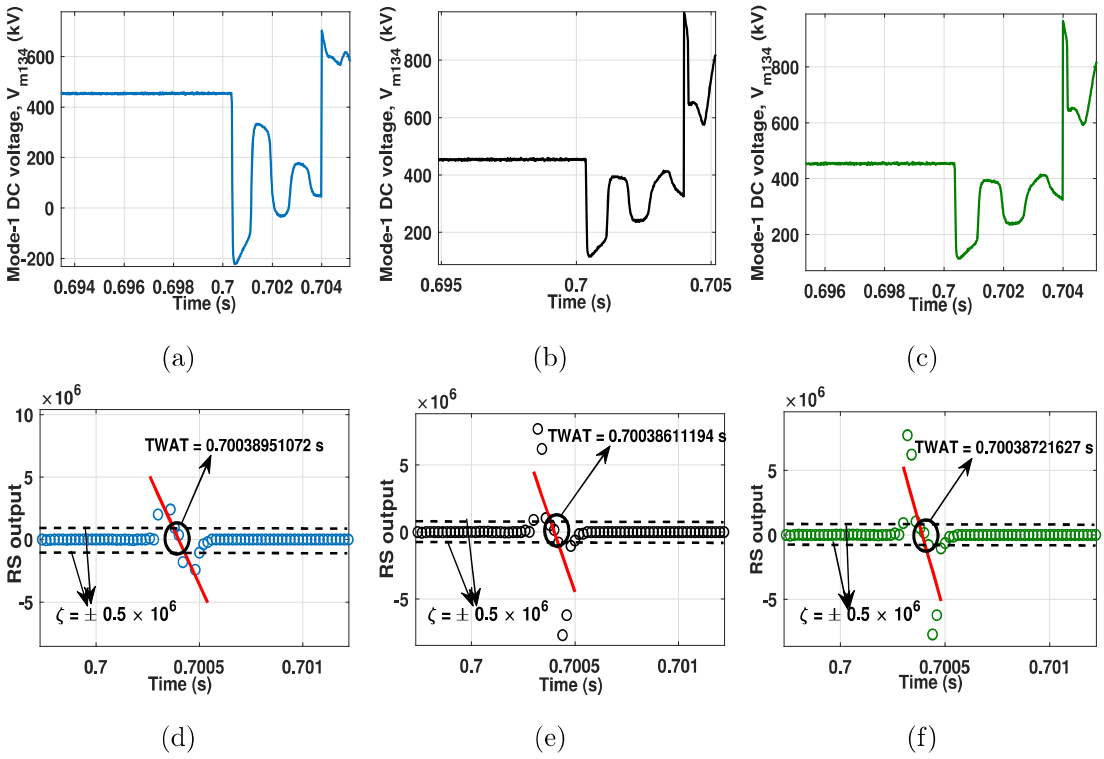


Figure 3.13: At DC terminal 3 (a) Mode-1 DC voltage with PPG fault, (b) Mode-1 DC voltage with PPG fault, (c) Mode-1 DC voltage with NPG fault, (d) TWAT detection for PP fault condition shown in (a), (e) TWAT detection for PPG fault condition shown in (b), (f) TWAT detection for NPG fault condition shown in (c).

respectively. The associated TWAT for different fault types are found to be 0.7003895 s, 0.7003861 s and 0.7003872 s for PPG, positive PG and negative PG fault respectively as shown in Fig. 3.13(d), (e) and (f). As evident form the proposed TWAT estimation performance shown in Fig. 3.13, it is consistent and insensitive to different fault type scenario.

To evaluate the performance of proposed TWAT based protection and DC fault localization scheme, the first incident TWAT estimation at DC terminal 3 and 4 are tabulated in Table 3.7 for different combination of fault type and fault location. From Table 3.7, it can be concluded that the proposed scheme accurately detects the internal fault and FLE is estimated to be within 0.740 % for different combination of fault types and locations, which infers that the proposed TW based protection and fault localization scheme is less sensitive to different fault types.

Table 3.7: Impact of fault type on proposed TW based DC protection and fault localization scheme

| AFL (km) | Fault type | AT of TW at DC terminal 3, $AT_{34}$ (s) | AT of TW at DC terminal 4, $AT_{43}$ (s) | FLE (%) | Internal Fault ($\lvert AT_{34} - AT_{43} \rvert$) $< \frac{l_{34}}{v_{TW}}$ |
|---|---|---|---|---|---|
| 20 | PPG | 0.70011618649 | 0.70102571930 | 0.731 | Yes |
| 20 | $+ve$ PG | 0.70011610534 | 0.70102668213 | 0.685 | Yes |
| 20 | $-ve$ PG | 0.70011591942 | 0.70102539213 | 0.734 | Yes |
| 70 | PPG | 0.70038951072 | 0.70072795201 | 0.388 | Yes |
| 70 | $+ve$ PG | 0.70038611194 | 0.70073160234 | 0.260 | Yes |
| 70 | $-ve$ PG | 0.70038721627 | 0.70072752091 | 0.307 | Yes |
| 130 | PPG | 0.70075280215 | 0.70041139230 | 0.259 | Yes |
| 130 | $+ve$ PG | 0.70075231958 | 0.70041221043 | 0.316 | Yes |
| 130 | $-ve$ PG | 0.70075341861 | 0.70041133726 | 0.230 | Yes |

### 3.4.6 Impact of external fault and MTDC grid parameter variation

To analyze the effect of external fault on the proposed TWAT based protection scheme, a PP fault (external fault to protective relay at DC substation 3 and 4) with 30 Ω fault resistance is simulated in DC cable $L_{24}$ at a distance of 10 km from DC substation 4. The mode-1 DC voltage waveform ($V_{m134}$) and extracted TWAT at DC terminal 3 and 4 is shown in Fig. 3.14. Similarly, the fault location at DC cable $L_{24}$ is changed to 20 km and 30 km, and the extracted TWAT is tabulated in Table 3.8. As evident form Table 3.8, the condition (3.20) is satisfied for the proposed TW based protection scheme which accurately identified the fault to be in external zone with respect to DC terminal 3 and 4. Therefore, it can be infer that the proposed TWAT based protection scheme is resilient to external fault and it can clearly discriminate between internal and external fault in the MTDC transmission system.

The grid parameter variations might also affect the DC protection scheme and there-

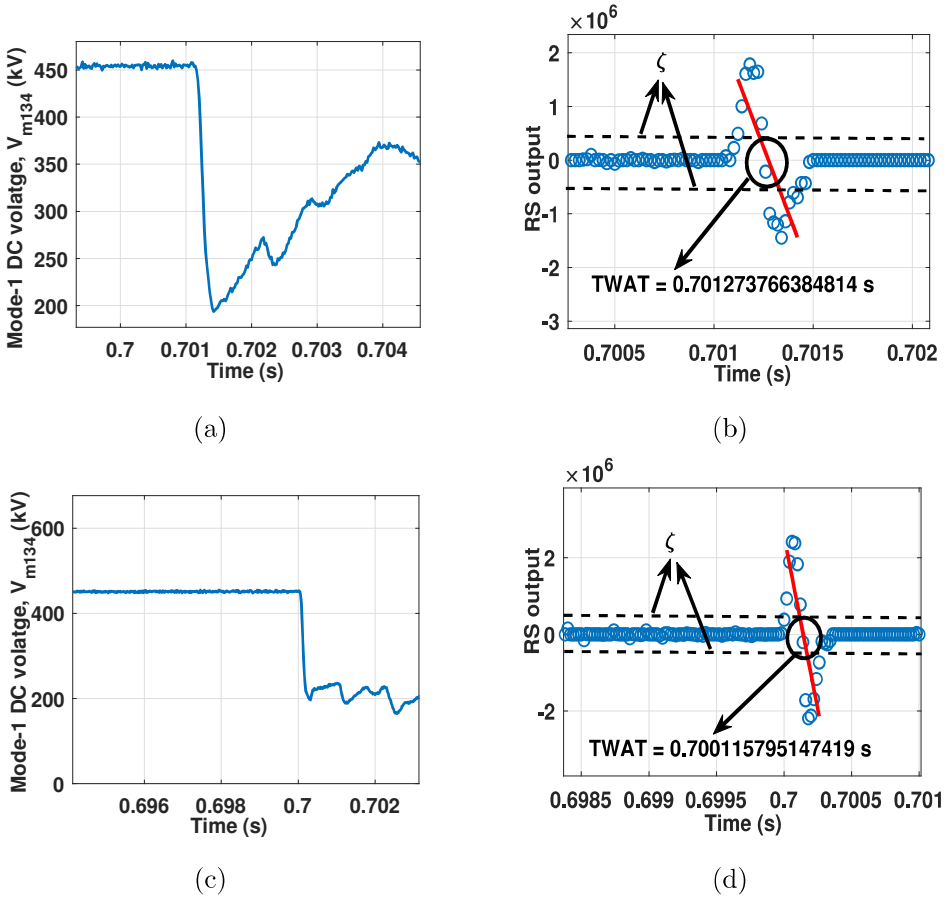


Figure 3.14: External fault at DC cable $L_{24}$ (a) Mode-1 DC voltage at DC terminal 3, (b) TWAT estimation by the proposed scheme at DC terminal 3, (c) Mode-1 DC voltage at DC terminal 4, (d) TWAT estimation by the proposed scheme at DC terminal 4.

fore it is necessary to evaluate the performance of the proposed TWAT based protection scheme against MTDC grid parameter variation such as active reference setting of MMC converter 4 [121]. The active power reference setting of MMC converter 4 is changed from 500 $MW$ to 150 $MW$ at 0.735 $s$ and the performance of proposed protection scheme is assessed under marge power order change as shown in Fig. 3.15. The transient at DC voltage waveform ($V_{43}$ with 35 dB measurement noise) at DC terminal 4 can be observed at 0.735 $s$ in Fig. 3.15(b). As evident from Fig. 3.15(c), the $RS$ output at the DC substation 4 does not exceeds the predetermined threshold $\zeta$ ($\pm 0.5 \times 10^6$) for the DC grid parameter variation, which indicates that the incident TW could not be considered as the fault induced TW and the proposed protection scheme will not be activated for the DC grid parameter changes.

Table 3.8: Impact of external fault and DC grid parameter variation on proposed TW based DC protection scheme

| Faulted cable | Fault location | AT of TW at DC terminal 3, $AT_{34}$ (s) | AT of TW at DC terminal 4, $AT_{43}$ (s) | $\frac{L_{34}}{v_{TW}}$ (ms) | External Fault ($\lvert AT_{34} - AT_{43} \rvert$) $= \frac{l_{34}}{v_{TW}} \pm 2\ \mu s$ |
|---|---|---|---|---|---|
| $L_{24}$ | 10 | 0.70127376639 | 0.70011579515 | 1.1581 | Yes |
| $L_{24}$ | 20 | 0.70133165453 | 0.70017168331 | 1.1581 | Yes |
| $L_{24}$ | 30 | 0.70138951630 | 0.70022954491 | 1.1581 | Yes |

### 3.4.7 Comparative assessment

#### 3.4.7.1 Comparing DC fault localization performance

In this section, the performance of proposed scheme is compared to the conventional MMG and S-transform based protection and fault localization scheme [36, 52]. To compare the performance of TW based fault location scheme, a PP fault with 100 Ω fault resistance is simulated in DC cable $L_{34}$ (under 35 dB SNR) at 70 km distance from DC substation 3. The MMG technique is applied to DC modal voltage ($V_{m134}, V_{m034}$ and $V_{m143}$) shown in Fig. 3.16(a) and the extracted TWAT for $V_{m134}$ and $V_{m143}$ are found to be 0.700420 s and 0.700700 s respectively as shown in Fig. 3.16(b) and Fig. 3.16(c). Finally, the estimated DC fault location and FLE using (3.21) and (3.22) for MMG based fault localization scheme is found to be 75.822 km and 2.911 % respectively. Similarly, S-transform technique is also used to extract TWAT from $V_{m134}$ under 35 dB noise contamination. But, as shown in Fig. 3.16(d), the S-transform technique could not differentiate between noise and TW arrival and fails to extract TWAT. Therefore, S-transform is used to estimate TWAT as 0.70042 $s$ and 0.70072 $s$ under 50 dB SNR for $V_{m134}$ and $V_{m143}$ respectively, which is shown in Fig. 3.16(e) and (f). The estimated DC fault location and FLE using (3.21) and (3.22) for S-transform based fault localization scheme is calculated to be 74.095 km and 2.047 % respectively for 50 dB SNR contaminated voltage signal.

Since FLE for the MMG and S-transform based DC fault location scheme under 50 kHz sampling frequency measurement is found to be 2.911 % and 2.047 % respectively,

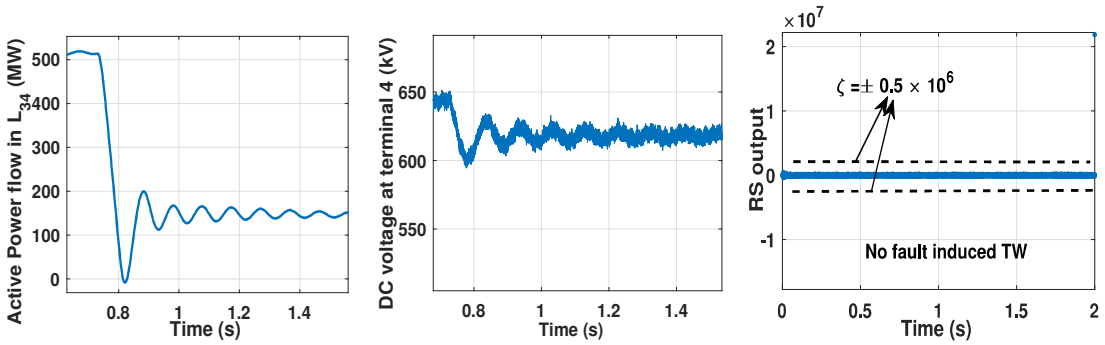


(a) (b) (c)

Figure 3.15: Impact of grid parameter changes (a) Abrupt change in active reference setting of MMC converter 4, (b) DC voltage waveform at DC terminal 4, (c) RS output at DC terminal 4 (no fault induced TW detection).

which is more than the required standard of 1 %. Due to low time resolution ($\Delta t$) of 20 $\mu s$, the maximum error in TWAT difference will be $\pm 2 \times \Delta t$ ($\pm 40 \mu s$) for MMG and S-transform based fault location scheme. Out of these, the S-transform based DC fault localization scheme fails to locate fault for DC voltage signal contaminated with 35 dB noise. On contrary, the proposed TWAT detection technique extracts the TWAT as 0.7003872215 s and 0.7007282745 s as shown in Fig. 3.16(h) and Fig. 3.16(i) respectively and the estimated DC fault location and FLE using (3.21) and (3.22) are 70.55 km and 0.275 % respectively for low sampling frequency (50 kHz) measurement. Therefore, it can be concluded that the proposed TW based Dc fault localization scheme could be compliant to IEC-61869-9 measurement standards, but MMG and S-Transform based techniques fails to estimate accurate DC fault location using low sampling frequency measurement and would not follow the measurement standard.

#### 3.4.7.2 Comparing DC primary protection performance

The MMG based protection scheme uses surge arrival time difference (SATD) between TW of mode-1 and mode-0 DC voltage signal at the local DC terminal [36]. But mode-0 DC voltage signal is absent for PPG fault, hence it can not be used to detect PPG fault by design [36]. To compare the performance of the proposed primary protection scheme with MMG based protection scheme [36], the same fault scenario is considered as in the previous subsection. The performance of conventional MMG and proposed TW based protection

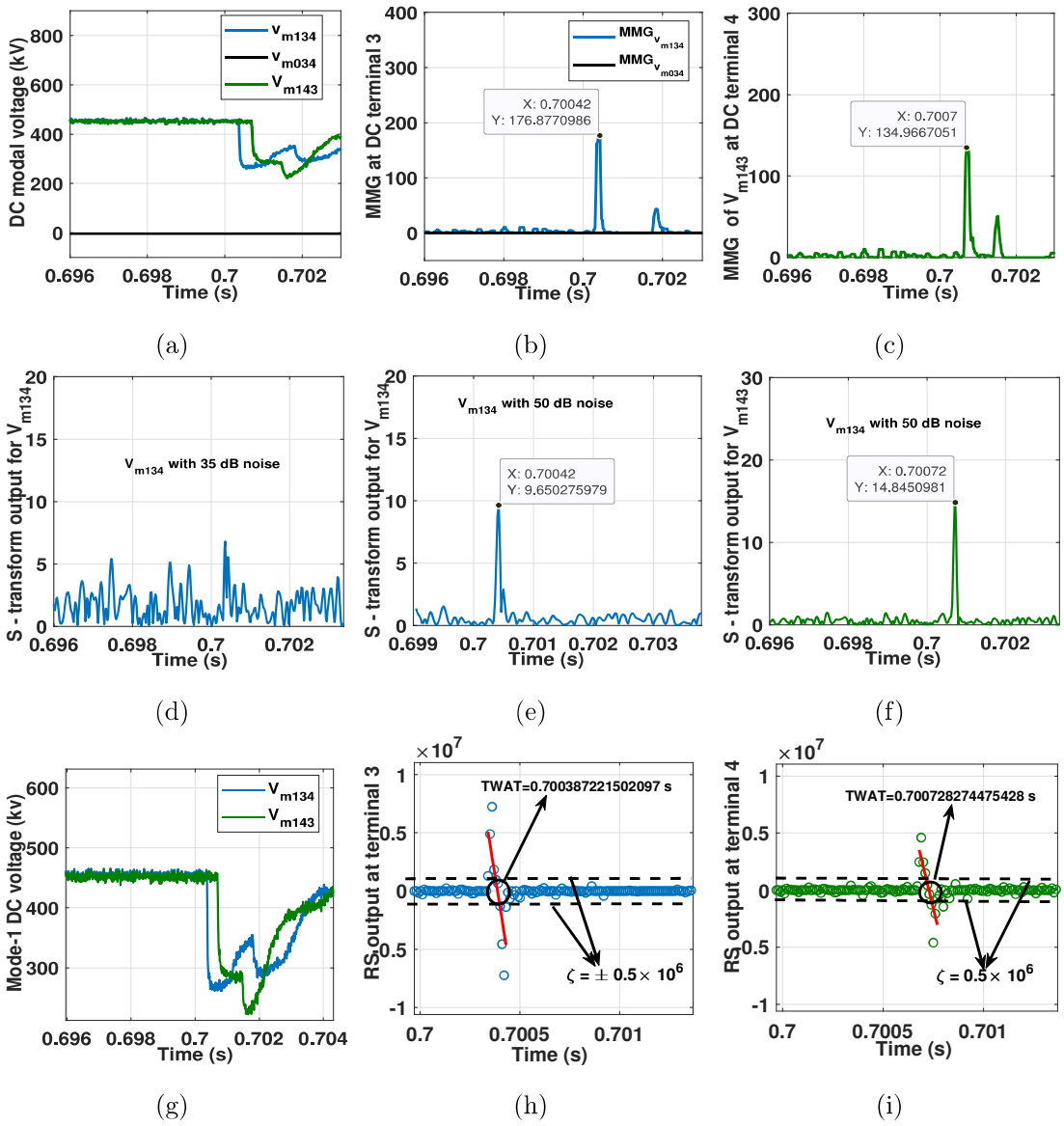


Figure 3.16: Comparison of proposed method with MMG and s-transform based protection and fault localization scheme (a) Mode-1 DC voltage at DC terminal 3 and 4 and mode-0 DC voltage at DC terminal 3, (b) TWAT estimation by MMG tool for modal signal in (a), (c) TWAT detection by MMG tool for mode-1 signal in (a), (d) No TW detection by S-transform output for modal signal in (a) under 35 dB noise, (e) TWAT estimation by S-transform output for modal signal in (a) under 50 dB noise, (f) TWAT estimation by S-transform output for modal signal in (a) under 50 dB noise, (h) Mode-1 DC voltage at DC terminal 3 and 4, (i) TWAT estimation for modal signal in (h) by proposed technique, (j) TWAT estimated for modal signal in (h) by proposed technique.

technique is shown in Fig. 3.16(b) and Fig. 3.16(g) & (h) respectively. As evident from Fig. 3.16(g) & (h), the proposed technique extracts the TWAT as 0.7003872215 s ($AT_{34}$) and 0.7007282745 s ($AT_{43}$) at DC terminal 3 and 4 respectively. The $|AT_{34} - AT_{43}|$ will be 0.341053 $ms$ which is less than TW propagation threshold 1.1581 $ms$ ($L_{34}/v_{TW}$) which satisfies (3.17) and the proposed scheme identifies the fault to be in internal zone. But, the MMG based DC protection scheme fails to detect TW in mode-0 DC voltage signal as shown in Fig. 3.16(b), which leads to non operation of SATD based DC protection scheme for PPG fault in MTDC grid. Moreover, the MMG based DC protection scheme proposed in [36] has suggested to use a minimum sampling frequency of 110 kHz, which restricts its compliance to IEC-61869-9 measurement standards for every fault scenarios.

### 3.4.8 Comparative discussion with existing DC protection system

The DC protection scheme proposed by ABB uses the pole-mode TW and its derivatives to detect the DC fault [122]. But its performance needs to be improved for high resistance fault and noise contaminated relaying signal. Similarly, SIEMENS has proposed a DC protection scheme based on the principle of TW integration, it improves the noise tolerance capability but slows the protective relaying speed [123]. Although, the DC protection scheme used by ABB and SIEMENS are compliant to IEC-61869-9 measurement standards with low sampling frequency requirement, but it can not be used for DC fault localization. On the other hand, the conventional TWAT based protection and fault localization scheme [49] requires high sampling frequency and data storage requirement, which makes it non-compliant to IEC-61869-9 measurement standards. To solve this issue, the TWAT based protection and fault localization scheme is proposed which is compliant to IEC-61869-9 measurement standard and it is also demonstrated to be robust against fault parameters, sampling frequency measurements, measurement noise and measurement error, grid parameter variation, communication delay and synchronization error.

The brief comparison of the proposed scheme against literature work is also tabulated in the following Table 3.9.

Table 3.9: Comparative analysis with existing protection and fault localization scheme

| **Fault location category** | **Features and challenges** |
|---|---|
| Travelling wave (TW) based | • Requirement of high sampling frequency measurements (500 kHz-1 MHz).<br>• Need for time-synchronized measurements (two-ended method).<br>• Non-compliant to IEC-61869-9 measurement standards.<br>• Training of the system is not required for TW based method. Therefore,it is highly reliable. |
| Machine Learning-based [5] | • Training of the system is required. Since fault records are not always sufficient (or sometimes not available at all) the training is usually implemented by simulation based iterative studies. This could raise concerns with regards to the reliability of the system training.<br>• Requirement of detailed system modelling, intensive training for different fault conditions, limited scalability, system topology dependence.<br>• Compliant to IEC-61869-9 measurement standards.<br>• It can not be principally categorized in TW based method. |
| Proposed technique (TW based) | • Requirement of low sampling frequency measurements (50 kHz).<br>• Training of the system is not required for TW based scheme. Therefore,it is highly reliable.<br>• Compliant to IEC-61869-9 measurement standards. |

## 3.5 Real time CHIL validation of proposed primary protection and DC fault localization scheme

To further back up the simulation results and assess the practical viability of the proposed scheme, a CHIL simulation testing has been performed. The RTDS is being used to emulate the behavior of CIGRE benchmark MTDC grid as shown in Fig. 3.17 [124]. The proposed primary protection and fault location method is implemented in TI TMS320F28379D digital signal processor (DSP) unit. The CHIL setup arrangement of RTDS and DSP (IED protection unit) unit is being shown in Fig. 3.18.

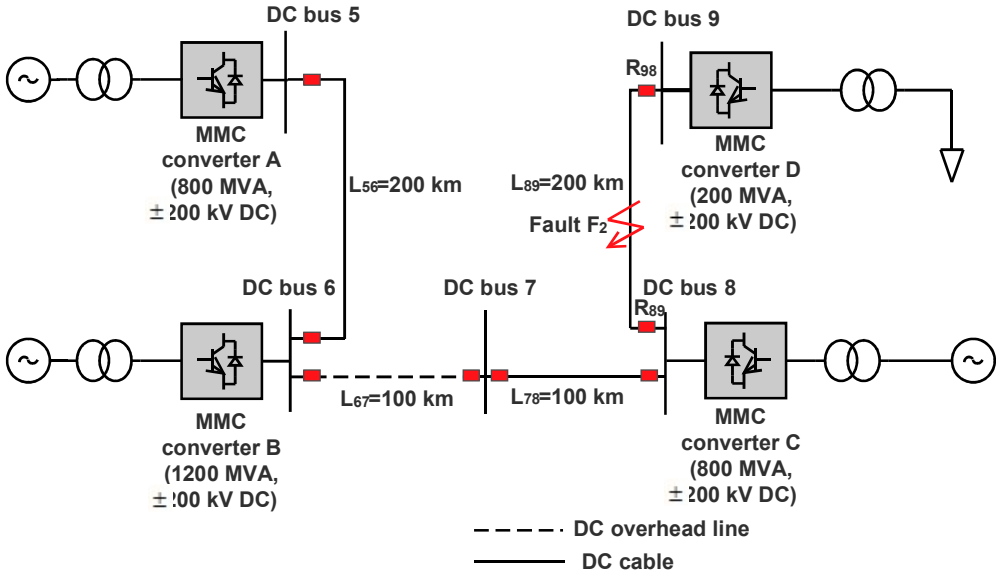


Figure 3.17: Four terminal symmetric monopole MTDC transmission system.

The DSP unit receives analog DC voltage signals (DC bus 8 and 9 voltage signals of CIGRE benchmark MTDC system) from giga-transceiver analog output (GTAO) card of the RTDS hardware unit at 50 kHz sampling frequency measurement. The input signals (positive pole and negative pole DC voltage from DC terminal 3 and 4 ($V_{34p}, V_{34n}, V_{43p}$ *and* $V_{43n}$)) extracted from GTAO cards are scaled down to fit the operating range of 16-bit analog to digital (ADC) converter of DSP unit (TMS320F28379D) i.e; 0-3.3 V as shown in Fig. 3.18(a). When the proposed protection and fault localization scheme modelled in TMS320F28379D platform detects the DC fault $F_2$, a digital trip signal is sent to HDCCB modelled in RTDS platform via giga-transceiver digital input (GTDI) card using general purpose input/output (GPIO) pin of TMS320F28379D

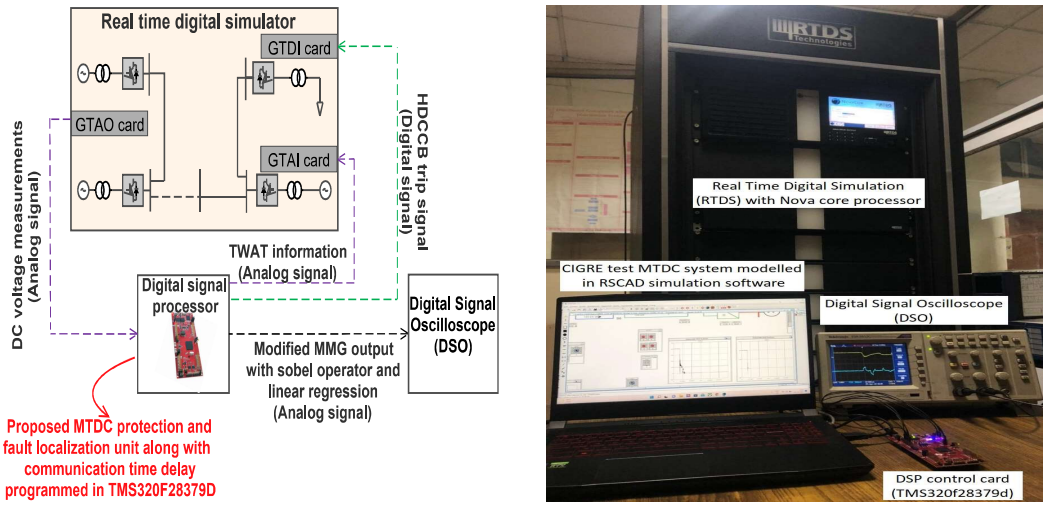


(a) (b)

Figure 3.18: (a) Schematic outline of CHIL test setup, (b) CHIL setup of RTDS and TI TMS320f28379D (IED) protection unit.

platform which is configured as digital input pin. Simultaneously, it also sends TWAT information at DC bus 8 and 9 to RTDS via giga-transceiver analog input (GTAI) card of RTDS and $RS(t)$ signal to digital signal oscilloscope (DSO) using 12-bit digital to analog converter (DAC) of TMS320F28379d platform, which is used for real time DC fault location as shown in Fig. 3.18(a).

For real time validation of the proposed primary protection and DC fault localization scheme under low sampling frequency (50 kHz) measurement, a DC fault $F_2$ with 10 Ω fault resistance is simulated in DC cable $L_{89}$ at 20 km distance from DC bus 8. The DSP platform emulates the behavior of proposed DC relay $R_{89}$ and $R_{98}$ at DC terminal 8 and 9 respectively. TMS320F28379D launchpad platform is hard wired connected to RTDS's I/O panel via ADC, DAC and GPIO module of TMS320F28379D processor board and it does not support IEC-61850-9-2 communication protocol. Therefore we have introduced a fixed communication delay of 1.33 $ms$ ($t_{comm}$ for 200 km optical fiber length) in the TMS320F28379D platform for practical real time validation. Fig. 3.19 shows the DC voltage profile at DC bus 8 and 9, and the RS output for the internal fault $F_2$ in DSO channel. The proposed protection scheme, emulated in DSP board, estimates the TWAT information at DC bus 8 and 9 to be 15.41044 s and 15.41123 s respectively as shown in Fig. 3.20(a) and (b), which is sent to the RTDS platform. The TW velocity is found

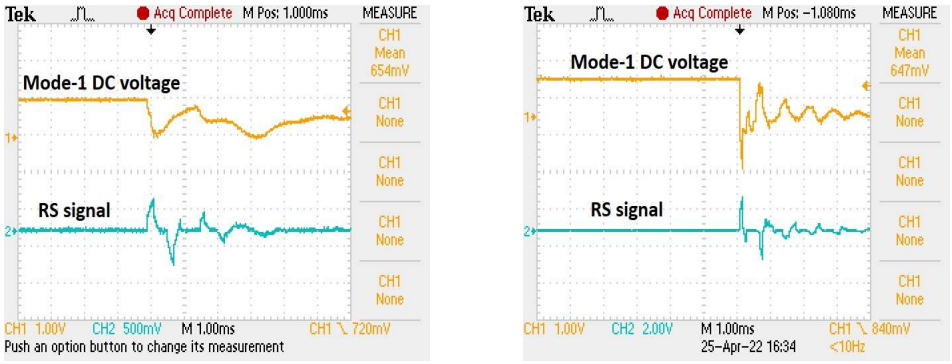


(a) (b)

Figure 3.19: (a) Mode-1 DC voltage and RS signal at DC terminal 8, (b) Mode-1 DC voltage and RS signal at DC terminal 9.

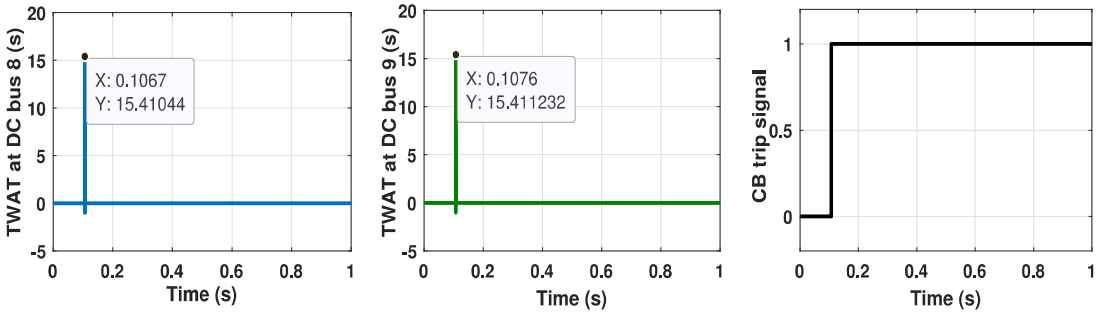


(a) (b) (c)

Figure 3.20: (a) AT of the first TW at DC terminal 8, (b) AT of the first TW at DC terminal 9, (C) CB trip signal sent to HDCCB located at DC cable between DC bus 8 and 9.

to be 198.5 $km/ms$ for the DC cable between DC terminal 8 and 9 for MTDC grid shown in Fig. 3.17. Since, the TWAT difference between DC bus 8 and 9 comes to be 0.792 ms ($|15.410440s - 15.411232s|$) which is less than the TW propagation threshold ($L_{89}/l_{TW} = 200/198.5\ km/ms = 1.007557\ ms$). Therefore, a DC relay trip signal is sent to associated HDCCB modelled in RTDS as shown in Fig. 3.20(c). Simultaneously, the proposed TW based DC fault localization estimates fault location to be 21.394 km using (3.21), and the FLE is found to be 0.697 % for low sampling frequency (50 kHz) measurement which makes it complaint to IEC-61869-9 measurement standard. Finally, the practical viability of the proposed TW based protection and real time fault location scheme is validated and its conformance to the measurement standard is provided with

the real time CHIL setup shown in Fig. 3.18(b).

## 3.6 Summary

Most of the conventional TW based MTDC protection schemes in the literature are non compliant to IEC 61869-9 measurement standard due to high sampling frequency (500 kHz-1 MHz) requirement. In this chapter, a novel double ended TW based primary protection and real time DC fault localization scheme is proposed, which is compliant to IEC 61869-9 measurement protocol. The proposed techniques uses modified MMG, sobel operator and linear regression tool to extract accurate AT from the fault induced TW under low sampling frequency (up to 50 kHz) measurement. The offline simulation conducted in PSCAD demonstrated the effectiveness of proposed protection and DC fault localization scheme against different fault resistance, fault location, sampling frequency, noise contaminated signal, time synchronization error, signal processing and communication delay. Finally, the practical feasibility of the proposed scheme has been demonstrated with the use of real time digital simulator and a low cost hardware prototype of IEDs using TI TMS320F28379D DSP board. The sensitive analysis of proposed algorithm is also summarized here -

1. The proposed TW based protection and fault localization scheme could detect and locate DC fault across different fault location on the DC transmission line, except the dead zone near DC terminal end (up to 1 km from both DC terminal end).

2. The performance of proposed protection and fault localization scheme is robust against measurement noise up to 35 dB.

3. The proposed TWAT estimation technique can efficiently estimate arrival time for the fault induced TW with fault impedance up to 200 Ω which ensures resilient fault detection and location for fault impedance up to 200 Ω.

4. the proposed protection scheme correctly identifies the internal fault and maximum fault location error is less than the allowable limit of 1 % for measurement error up to 1 %.

5. The proposed scheme could efficiently detect and locate fault for sampling frequency up to 50 kHz, making it compliant to IEC-61869-9 measurement standard.

6. The total time delay introduced by the proposed protection scheme, which incorporates processing time of TW based AT estimation technique, communication delay and HDCCB opening delay, will be 3.66 ms which is less than the required time frame of 5 ms for MTDC primary protection scheme.

7. The proposed scheme uses IEC-61588 PTP protocol which ensures maximum $\delta t_s yn$ of 50 ns, its performance is evaluated for $\delta t_s yn$ up to 5 $\mu s$ and estimated fault location error lies within 1 %.

8. The proposed scheme accurately detects the internal fault and FLE is estimated to be within 0.740 % for different combination of fault types and locations, which infers that the proposed TW based protection and fault localization scheme is less sensitive to different fault types.

9. The relaying signal (RS) output at the DC substation do not exceeds the predetermined threshold $\zeta$ ($\pm 0.510^6$) for the DC grid parameter variation, which indicates that the incident TW could not be considered as the fault induced TW and the proposed protection scheme will not be activated for the DC grid parameter changes.

10. The proposed TWAT based protection scheme is resilient to external fault and it can clearly discriminate between internal and external fault in the MTDC transmission system.